LINEAR MODE CONNECTIVITY IN DIFFERENTIABLE TREE ENSEMBLES

Anonymous authors
Paper under double-blind review

ABSTRACT

Linear Mode Connectivity (LMC) refers to the phenomenon that performance remains consistent for linearly interpolated models in the parameter space. For independently optimized model pairs from different random initializations, achieving LMC is considered crucial for understanding the stable success of the non-convex optimization in modern machine learning models and for facilitating practical parameter-based operations such as model merging. While LMC has been achieved for neural networks by considering the permutation invariance of neurons in each hidden layer, its attainment for other models remains an open question. In this paper, we first achieve LMC for *soft tree ensembles*, which are tree-based differentiable models extensively used in practice. We show the necessity of incorporating two invariances: *subtree flip invariance* and *splitting order invariance*, which do not exist in neural networks but are inherent to tree architectures, in addition to permutation invariance of trees. Moreover, we demonstrate that it is even possible to exclude such additional invariances while keeping LMC by designing *decision list*-based tree architectures, where such invariances do not exist by definition. Our findings indicate the significance of accounting for architecture-specific invariances in achieving LMC.

1 INTRODUCTION

A non-trivial empirical characteristic of modern machine learning models trained using gradient methods is that models trained from different random initializations could achieve nearly identical performance, even though their parameter representations differ. If the outcomes of all training sessions converge to the same local minima, this empirical phenomenon can be understood. However, considering the complex non-convex nature of the loss surface, the optimization results are unlikely to converge to the same local minima. In recent years, particularly within the context of neural networks, the transformation of model parameters while preserving functional equivalence has been explored by considering the *permutation invariance* of neurons in each hidden layer (Hecht-Nielsen, 1990; Chen et al., 1993). Notably, only a slight performance degradation has been observed when using weights derived through linear interpolation between permuted parameters obtained from different training processes (Entezari et al., 2022; Ainsworth et al., 2023). This demonstrates that the trained models reside in different, yet equivalent, local minima. This situation is referred to as *Linear Mode Connectivity* (LMC) (Frankle et al., 2020). From a theoretical perspective, LMC is crucial for understanding the stable and successful application of non-convex optimization. As noted by Entezari et al. (2022) and Ainsworth et al. (2023), achievement of LMC suggests that loss landscapes often contain (nearly) a single basin after accounting for all possible invariances, which can be an intuitive reason for the robustness of gradient methods to different random initialization and data batch orders. In addition, LMC also holds significant practical importance, enabling techniques such as model merging (Wortsman et al., 2022; Ortiz-Jimenez et al., 2023) by weight-space parameter averaging.

Although neural networks are most extensively studied among the models trained using gradient methods, other models also thrive in real-world applications. A representative is decision tree ensemble models, such as random forests (Breiman, 2001). A decision tree ensemble makes predictions by combining the outputs of multiple trees that recursively split the data into subsets at each node and make final predictions at their leaves. While they are originally trained by not gradient but greedy algorithms, their *differentiable* variant, called *soft tree ensembles*, which learn parameters of the entire model through gradient-based optimization, have recently been actively studied. Not only

empirical studies regarding accuracy and interpretability (Popov et al., 2020; Hazimeh et al., 2020; Chang et al., 2022), but also theoretical analyses have been performed (Kanoh & Sugiyama, 2022; 2023). Moreover, the differentiability of soft trees allows for integration with various deep learning methodologies, including fine-tuning (Ke et al., 2019), dropout (Srivastava et al., 2014), and various stochastic gradient descent methods (Kingma & Ba, 2015; Foret et al., 2021). Furthermore, the soft tree represents the most elementary form of a hierarchical mixture of experts (Jordan & Jacobs, 1993; Shazeer et al., 2017; Lepikhin et al., 2021). Investigating soft tree models not only advances our understanding of this particular structure but also contributes to broader research into essential technological components critical for the development of large-scale models (Jiang et al., 2024).

A research question that we tackle in this paper is: "Can LMC be achieved for soft tree ensembles?". While achieving LMC has advanced the understanding of non-convex optimization and the use of model merging in neural networks, it has yet to be explored in tree ensemble models. The reasons behind achieving LMC, even in neural networks, are not fully understood, and whether LMC can be realized in soft tree ensembles, given their distinct architectures, is also unclear. Thus, our contribution of examining LMC in soft tree ensembles provides not only novel insights and techniques for tree ensemble models but also broadens the understanding of the LMC phenomenon by introducing perspectives beyond neural networks for the first time.

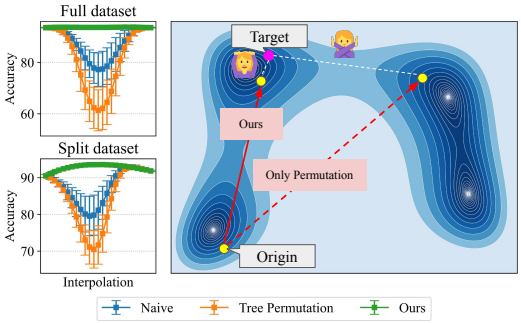

Figure 1: A representative experimental result on the MiniBooNE (Roe, 2010) dataset (left) and conceptual diagram of LMC for tree ensembles (right).

Our results, which are highlighted with a green line in the top left panel of Figure 1, clearly show that the answer to our research question is "Yes". This plot shows the variation in test accuracy when interpolating weights of soft oblivious trees, perfect binary soft trees with shared parameters at each depth, trained from different random initializations. The green line is obtained by our method introduced in this paper, where there is almost zero performance degradation. Furthermore, as shown in the bottom left panel of Figure 1, the performance can even improve when interpolating between models trained on split datasets.

The key insight is that, when performing interpolation between two model parameters, considering only tree permutation invariance, which corresponds to the permutation invariance of neural networks, is *not sufficient* to achieve LMC, as shown in the orange lines in the plots. An intuitive understanding of this situation is also illustrated in the right panel of Figure 1. To achieve LMC, that is, the green lines, we show that two additional invariances beyond tree permutation, *subtree flip invariance* and *splitting order invariance*, which inherently exist for tree architectures, should be accounted for.

Moreover, we demonstrate that it is possible to exclude such additional invariances while preserving LMC by modifying tree architectures. We realize such an architecture based on *a decision list*, a binary tree structure where branches extend in only one direction. By designating one of the terminal leaves as an empty node, we introduce a customized decision list that omits both subtree flip invariance and splitting order invariance, and empirically show that this can achieve LMC by considering only tree permutation invariance. Since incorporating additional invariances is computationally expensive, we can efficiently perform weight-space averaging in model merging on our customized decision lists.

Our contributions are summarized as follows:

- First achievement of LMC for tree ensembles with additional invariances beyond tree permutation.
- Development of a decision list-based architecture that does not involve additional invariances.
- A thorough empirical investigation of LMC across various tree architectures, invariances, and real-world datasets.

2 Preliminary

We prepare the basic concepts of LMC and soft tree ensembles.

2.1 LINEAR MODE CONNECTIVITY

Let us consider two models, A and B, that have the same architecture. In the context of evaluating LMC, the concept of a "barrier" is frequently used (Ainsworth et al., 2023; Guerrero Peña et al., 2023). Let $\boldsymbol{\Theta}_A$ and $\boldsymbol{\Theta}_B$ be parameters of models A and B, respectively. Their shapes can be defined arbitrarily. In this paper, for tree ensemble models, $\boldsymbol{\Theta}_A, \boldsymbol{\Theta}_B \in \mathbb{R}^{M \times P}$ for the number P of parameters per tree and the number M of trees. Assume that $\mathcal{C} : \mathbb{R}^{M \times P} \to \mathbb{R}$ measures the performance of the model, such as accuracy. If higher values of $\mathcal{C}(\cdot)$ mean better performance, the barrier between two parameter vectors $\boldsymbol{\Theta}_A$ and $\boldsymbol{\Theta}_B$ is defined as:

$$\mathcal{B}(\boldsymbol{\Theta}_A, \boldsymbol{\Theta}_B) = \sup_{\lambda \in [0,1]} \left[\lambda \mathcal{C}(\boldsymbol{\Theta}_A) + (1-\lambda)\mathcal{C}(\boldsymbol{\Theta}_B) - \mathcal{C}(\lambda \boldsymbol{\Theta}_A + (1-\lambda)\boldsymbol{\Theta}_B) \right]. \tag{1}$$

We can simply reverse the subtraction order if lower values of $\mathcal{C}(\cdot)$ mean better performance like loss.

Several techniques have been developed to reduce barriers by transforming parameters while preserving functional equivalence. Two main approaches are *activation matching* (AM) and *weight matching* (WM). AM takes the behavior of model inference into account, while WM simply compares two models using their parameters. The validity of both AM and WM has been theoretically supported by Zhou et al. (2023). Numerous algorithms are available for implementing AM and WM. For instance, Ainsworth et al. (2023) uses a formulation based on the Linear Assignment Problem (LAP), also known as finding the minimum-cost matching in bipartite graphs, to determine suitable permutations. Guerrero Peña et al. (2023) employs a differentiable formulation that allows for the optimization of permutations using gradient-based methods.

Existing research has focused exclusively on neural networks such as multi-layer perceptrons (MLP) and convolutional neural networks (CNN). No study has been conducted for soft tree ensembles.

2.2 SOFT TREE ENSEMBLE

Unlike typical hard decision trees, which explicitly determine the data flow to the right or left at each splitting node, soft trees represent the proportion of data flowing to the right or left as continuous values between 0 and 1. This approach enables a differentiable formulation. We use a sigmoid function, $\sigma : \mathbb{R} \to (0,1)$ to formulate a function $\mu_{m,\ell}(\boldsymbol{x}_i, \boldsymbol{w}_m, \boldsymbol{b}_m) : \mathbb{R}^F \times \mathbb{R}^{F \times \mathcal{N}} \times \mathbb{R}^{1 \times \mathcal{N}} \to (0,1)$ that represents the proportion of the ith data point $\boldsymbol{x}_i$ flowing to the ℓth leaf of the mth tree as a result of soft splittings:

$$\mu_{m,\ell}(\boldsymbol{x}_i, \boldsymbol{w}_m, \boldsymbol{b}_m) = \prod_{n=1}^{\mathcal{N}} \underbrace{\sigma(\boldsymbol{w}_{m,n}^\top \boldsymbol{x}_i + b_{m,n})}_{\text{flow to the left}}^{\mathbb{1}_{\ell \swarrow n}} \underbrace{(1 - \sigma(\boldsymbol{w}_{m,n}^\top \boldsymbol{x}_i + b_{m,n}))}_{\text{flow to the right}}^{\mathbb{1}_{n \searrow \ell}}, \tag{2}$$

where $\mathcal{N}$ denotes the number of splitting nodes in each tree. The parameters $\boldsymbol{w}_{m,n} \in \mathbb{R}^F$ and $b_{m,n} \in \mathbb{R}$ correspond to the feature selection mask and splitting threshold value for nth node in a mth tree, respectively. The expression $\mathbb{1}_{\ell \swarrow n}$ (resp. $\mathbb{1}_{n \searrow \ell}$) is an indicator function that returns 1 if the ℓth leaf is positioned to the left (resp. right) of a node n, and 0 otherwise.

If parameters are shared across all splitting nodes at the same depth, such perfect binary trees are called *oblivious trees*. Mathematically, $\boldsymbol{w}_{m,n} = \boldsymbol{w}_{m,n'}$ and $b_{m,n} = b_{m,n'}$ for any nodes n and n' at the same depth in an oblivious tree. Oblivious trees can significantly reduce the number of parameters from an exponential to a linear order of the tree depth, and they are actively used in practice (Popov et al., 2020; Chang et al., 2022).

To classify C categories, the output of the mth tree is computed by the function $f_m : \mathbb{R}^F \times \mathbb{R}^{F \times \mathcal{N}} \times \mathbb{R}^{1 \times \mathcal{N}} \times \mathbb{R}^{C \times \mathcal{L}} \to \mathbb{R}^C$ as sum of the leaves $\boldsymbol{\pi}_{m,\ell}$ weighted by the outputs of $\mu_{m,\ell}(\boldsymbol{x}_i, \boldsymbol{w}_m, \boldsymbol{b}_m)$:

$$f_m(\boldsymbol{x}_i, \boldsymbol{w}_m, \boldsymbol{b}_m, \boldsymbol{\pi}_m) = \sum_{\ell=1}^{\mathcal{L}} \mu_{m,\ell}(\boldsymbol{x}_i, \boldsymbol{w}_m, \boldsymbol{b}_m) \boldsymbol{\pi}_{m,\ell}, \tag{3}$$

where $\mathcal{L}$ is the number of leaves in a tree. To facilitate understanding, the formulation for tree depth is $D = 1$ is illustrated in Figure 2.

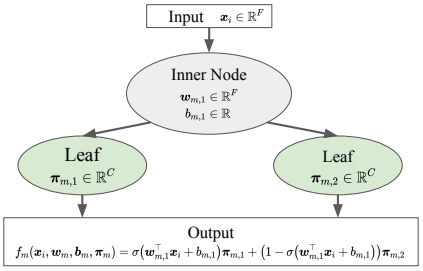

Figure 2: A soft decision tree with a single inner node and two leaf nodes.

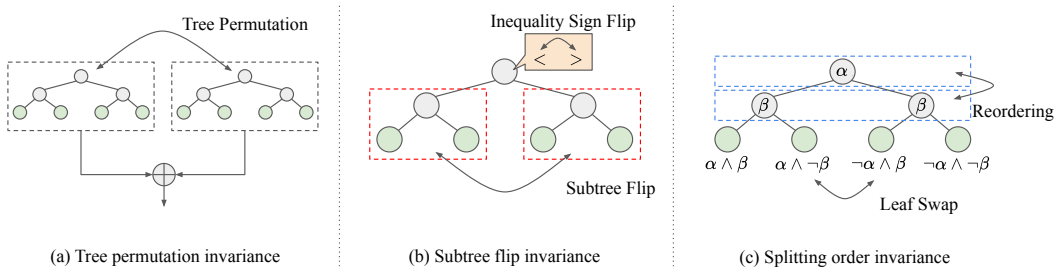

(a) Tree permutation invariance (b) Subtree flip invariance (c) Splitting order invariance

Figure 3: Invariances inherent to tree ensembles.

If $\mu_{m,\ell}(\boldsymbol{x}_i, \boldsymbol{w}_m, \boldsymbol{b}_m)$ takes the value of 1.0 for one leaf and 0.0 for the others, the leaf value itself becomes the prediction output, making the model behavior equivalent to that of a standard oblique decision tree (Murthy et al., 1994).

By combining this function for M trees, we realize the function $f : \mathbb{R}^F \times \mathbb{R}^{M \times F \times \mathcal{N}} \times \mathbb{R}^{M \times 1 \times \mathcal{N}} \times \mathbb{R}^{M \times C \times \mathcal{L}} \to \mathbb{R}^C$ as an ensemble model consisting of M trees:

$$f(\boldsymbol{x}_i, \boldsymbol{w}, \boldsymbol{b}, \boldsymbol{\pi}) = \sum_{m=1}^{M} f_m(\boldsymbol{x}_i, \boldsymbol{w}_m, \boldsymbol{b}_m, \boldsymbol{\pi}_m), \tag{4}$$

with the trainable parameters $\boldsymbol{w} = (\boldsymbol{w}_1, \ldots, \boldsymbol{w}_M)$, $\boldsymbol{b} = (\boldsymbol{b}_1, \ldots, \boldsymbol{b}_M)$, and $\boldsymbol{\pi} = (\boldsymbol{\pi}_1, \ldots, \boldsymbol{\pi}_M)$ being randomly initialized.

As shown in Equation 4, tree ensembles exhibit permutation invariance when the order of the M trees is rearranged, similar to the permutation invariance observed in the hidden neurons of neural networks. However, as discussed in the next section, tree ensembles exhibit several other types of invariance beyond permutation, setting their behavior apart from that of neural networks. In addition to these invariances, there are several key differences between tree ensembles and neural networks. Due to the hierarchical binary tree structure, the influence of each node parameter on the overall model depends on its node position. Moreover, unlike neural networks, tree ensembles lack the concept of activation and intermediate layers. These factors make it challenging to directly apply the matching strategies used for neural networks to achieve LMC.

3 Invariances Inherent to Tree Ensembles

In this section, we discuss additional invariances inherent to trees (Section 3.1) and introduce a matching strategy specifically for tree ensembles (Section 3.2). We also show that the presence of additional invariances varies depending on the tree structure, and we present tree structures where no additional invariances beyond tree permutation exist (Section 3.3).

3.1 Parameter Modification Processes

When we consider perfect binary trees, there are three types of invariance:

- **Tree permutation invariance.** In Equation 4, the behavior of the function does not change even if the order of the M trees is altered, as shown in Figure 3(a). This corresponds to the permutation of hidden neurons in neural networks, which has been a subject in previous studies on LMC.
- **Subtree flip invariance.** When the left and right subtrees are swapped simultaneously with the inversion of the inequality sign at the split, the functional behavior remains unchanged, which we refer to *subtree flip invariance*. Figure 3(b) presents a schematic diagram of this invariance, which is not found in neural networks but is unique to binary tree-based models. Since $\sigma(-c) = 1 - \sigma(c)$ for $c \in \mathbb{R}$ due to the symmetry of $\mathrm{sigmoid}$, the inversion of the inequality is achieved by inverting the signs of $\boldsymbol{w}_{m,n}$ and $b_{m,n}$. Yadav et al. (2023) also focused on the sign of weights, but in a different way from ours. They pay attention to the amount of change from the parameters at the start of fine-tuning, rather than discussing the sign of the parameters.

- **Splitting order invariance.** Oblivious trees share parameters at the same depth, which means that the decision boundaries are straight lines without any bends. With this characteristic, even if the splitting rules at different depths are swapped, functional equivalence can be achieved if the positions of leaves are also swapped appropriately as shown in Figure 3(c). This invariance does not exist for non-oblivious perfect binary trees without parameter sharing, as the behavior of the decision boundary varies depending on the splitting order.

Note that MLPs also have an additional invariance beyond just permutation. Particularly in MLPs that employ ReLU as an activation function, the output of each layer changes linearly with a zero crossover. Therefore, it is possible to modify parameters without changing functional behavior by multiplying the weights in one layer by a constant and dividing the weights in the previous layer by the same constant. However, since the soft tree is based on the $\mathrm{sigmoid}$ function, this invariance does not apply. Previous studies (Entezari et al., 2022; Ainsworth et al., 2023; Guerrero Peña et al., 2023) have consistently achieved significant reductions in barriers without accounting for this scale invariance. One potential reason is that changes in parameter scale are unlikely due to the nature of optimization via gradient descent. Conversely, when we consider additional invariances inherent to trees, the scale is equivalent to the original parameters.

3.2 Matching Strategy

When considering subtree flip invariance and splitting order invariance, it is necessary to compare multiple functionally equivalent trees and select the most suitable one for achieving LMC. Although comparing tree parameters is a straightforward approach, since the contribution of all the parameters in a tree is not equal, we apply appropriate weighting for each node. By interpreting a tree as a rule set with shared parameters as shown in Figure 4, we determine the weight of each splitting node by counting the number of leaves to which the node affects. For example, in the case of the left example in Figure 4, the root node affects eight leaves, nodes at depth 2 affect four leaves, and nodes at depth 3 affect two leaves. This strategy can apply to even trees other than perfect binary trees. For example, in the right example of Figure 4, the root node affects four leaves, a node at depth 2 affects three leaves, and a node at depth 3 affects two leaves.

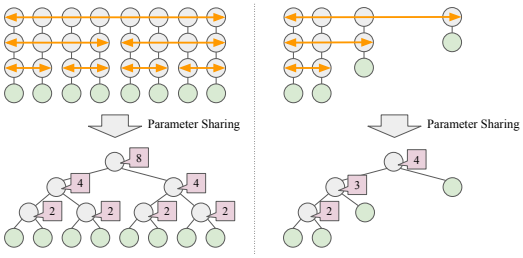

Figure 4: Weighting strategy.

Using the weighting operation described above, we present the straightforward matching procedure in Algorithms 1 and 2. We perform an exhaustive search to explore all patterns with subtree flip invariance and splitting order invariance, while handling tree permutation invariance with the LAP. We treat the output of each individual tree like the activation value of a neural network in the case of AM. Note that although it is necessary to solve the LAP multiple times for each layer in MLPs to perform coordinate descent (Ainsworth et al., 2023), tree ensembles require only a single run of the LAP since there is no concept of intermediate layers.

Notations used in Algorithms 1 and 2. Multidimensional array elements are accessed using square brackets $[\cdot]$. For example, for $\boldsymbol{G} \in \mathbb{R}^{I \times J}$, $\boldsymbol{G}[i]$ refers to the ith slice along the first dimension, and $\boldsymbol{G}[:, j]$ refers to the jth slice along the second dimension, with sizes $\mathbb{R}^J$ and $\mathbb{R}^I$, respectively. Furthermore, it can also accept a vector $\boldsymbol{v} \in \mathbb{N}^l$ as an input. In this case, $\boldsymbol{G}[\boldsymbol{v}] \in \mathbb{R}^{l \times J}$. The Flatten function converts multidimensional input into a one-dimensional vector format. As the LinearSumAssignment function, $\mathrm{scipy.optimize.linear_sum_assignment}$[1] is used to solve the LAP. In the AdjustTree function, the parameters of a tree are modified according to the uth pattern among the enumerated $U \in \mathbb{N}$ total additional invariances patterns. Additionally, in the Weighting function, parameters are multiplied by the square root of their weights to simulate the process of assessing a rule set. If the first argument for the UpdateBestOperation function, the input inner product, is larger than any previously input inner product values, then u' is updated with u, the second argument. If not, u' remains unchanged.

[1] https://docs.scipy.org/doc/scipy/reference/generated/scipy.optimize.linear_sum_assignment.html

Algorithm 1: Activation matching for soft tree ensembles

ActivationMatching($\boldsymbol{\Theta}_A \in \mathbb{R}^{M \times P}$, $\boldsymbol{\Theta}_B \in \mathbb{R}^{M \times P}$, $\boldsymbol{x}_{\text{sampled}} \in \mathbb{R}^{F \times N_{\text{sampled}}}$)
  Initialize $\boldsymbol{O}_A \in \mathbb{R}^{M \times N_{\text{sampled}} \times C}$ and $\boldsymbol{O}_B \in \mathbb{R}^{M \times N_{\text{sampled}} \times C}$ to store outputs
  for $m = 1$ *to* M **do**
    for $i = 1$ *to* N_{sampled} **do**
      Set the output of the mth tree with $\boldsymbol{\Theta}_A[m]$ using $\boldsymbol{x}_{\text{sampled}}[:, i]$ to $\boldsymbol{O}_A[m, i]$.
      Set the output of the mth tree with $\boldsymbol{\Theta}_B[m]$ using $\boldsymbol{x}_{\text{sampled}}[:, i]$ to $\boldsymbol{O}_B[m, i]$.
  Initialize similarity matrix $\boldsymbol{S} \in \mathbb{R}^{M \times M}$
  for $m_A = 1$ *to* M **do**
    for $m_B = 1$ *to* M **do**
      $\boldsymbol{S}[m_A, m_B] \leftarrow \text{Flatten}(\boldsymbol{O}_A[m_A]) \cdot \text{Flatten}(\boldsymbol{O}_B[m_B])$
  $\boldsymbol{p} \leftarrow \text{LinearSumAssignment}(\boldsymbol{S})$ // $\boldsymbol{p} \in \mathbb{N}^M$: Optimal assignments
  $\boldsymbol{\Theta}_A, \boldsymbol{\Theta}_B \leftarrow \text{Weighting}(\boldsymbol{\Theta}_A, \boldsymbol{\Theta}_B)$
  Initialize operation indices $\boldsymbol{q} \in \mathbb{N}^M$
  for $m = 1$ *to* M **do**
    for $u = 1$ *to* U **do** // $U \in \mathbb{N}$: Number of possible operations
      $u' \leftarrow \text{UpdateBestOperation}(\text{AdjustTree}(\boldsymbol{\Theta}_A[m], u) \cdot \boldsymbol{\Theta}_B[m], u)$
    Append u' to $\boldsymbol{q}$ // $\boldsymbol{q} \in \mathbb{N}^M$: Optimal operations
  return $\boldsymbol{p}, \boldsymbol{q}$

Algorithm 2: Weight matching for soft tree ensembles

WeightMatching($\boldsymbol{\Theta}_A \in \mathbb{R}^{M \times P}$, $\boldsymbol{\Theta}_B \in \mathbb{R}^{M \times P}$)
  $\boldsymbol{\Theta}_A, \boldsymbol{\Theta}_B \leftarrow \text{Weighting}(\boldsymbol{\Theta}_A, \boldsymbol{\Theta}_B)$
  Initialize similarity matrix for each operation $\boldsymbol{S} \in \mathbb{R}^{U \times M \times M}$
  for $u = 1$ *to* U **do** // $U \in \mathbb{N}$: Number of possible operations
    for $m_A = 1$ *to* M **do**
      $\boldsymbol{\theta} \leftarrow \text{AdjustTree}(\boldsymbol{\Theta}_A[m_A], u)$ // $\boldsymbol{\theta} \in \mathbb{R}^P$: Adjusted tree-wise parameters
      for $m_B = 1$ *to* M **do**
        $\boldsymbol{S}[u, m_A, m_B] \leftarrow \boldsymbol{\theta} \cdot \boldsymbol{\Theta}_B[m_B]$
  $\boldsymbol{S}' \leftarrow \max(\boldsymbol{S}, \text{axis=0})$ // $\boldsymbol{S}' \in \mathbb{R}^{M \times M}$: Similarity matrix between trees
  $\boldsymbol{p} \leftarrow \text{LinearSumAssignment}(\boldsymbol{S}')$ // $\boldsymbol{p} \in \mathbb{N}^M$: Optimal assignments
  $\boldsymbol{q} \leftarrow \text{argmax}(\boldsymbol{S}, \text{axis=0})[\boldsymbol{p}]$ // $\boldsymbol{q} \in \mathbb{N}^M$: Optimal operations
  return $\boldsymbol{p}, \boldsymbol{q}$

Complexity. The time complexity of solving the LAP is $\mathcal{O}(M^3)$ using a modified Jonker-Volgenant algorithm without initialization (Crouse, 2016), where M is the number of trees. This process needs to be performed only once in both WM and AM to consider tree permutation invariance. However, the number of additional invariance patterns U scales rapidly as D increases. In a non-oblivious perfect binary tree with depth D, there are $2^D - 1$ splitting nodes, resulting in 2^{2^D-1} possible combinations of sign flips, giving total additional invariances pattern $U = 2^{2^D-1}$. Additionally, in the case of oblivious trees with depth D, the number of splitting rules that consider sign flipping is reduced from 2^{2^D-1} to 2^D due to the splitting rule sharing at the same depth, and considering the $D!$ distinct splitting order invariance patterns, we have $U = 2^D D!$. Therefore, for large values of D, conducting an exhaustive search to consider additional invariances becomes impractical.

In Section 3.3, we will discuss methods to eliminate additional invariance by adjusting the tree structure. This enables efficient matching even for deep models. Additionally, in Section 4.2, we will present numerical experiment results and discuss that the practical motivation to apply these algorithms is limited when targeting deep perfect binary trees.

3.3 ARCHITECTURE-DEPENDENCY OF THE INVARIANCES

In Section 3.1, we focused on perfect binary trees as they are most commonly used in soft trees (Frosst & Hinton, 2017; Popov et al., 2020; Hazimeh et al., 2020). However, tree architectures can be flexible, and we show that we can specifically design architecture that has neither subtree flip nor splitting order invariances. This allows efficient matching as considering such two invariances is computationally expensive.

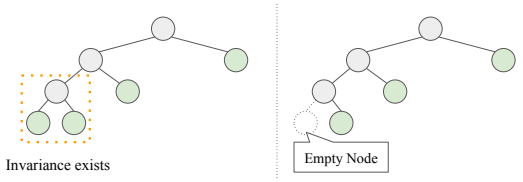

Figure 5: Tree architecture where neither subtree flip invariance nor splitting order invariance exists.

Table 1: Invariances inherent to each model architecture.

	Perm	**Flip**	**Order**
Non-Oblivious Tree	✓	✓	×
Oblivious Tree	✓	✓	✓
Decision List	✓	(✓)	×
Decision List (Modified)	✓	×	×

Our idea is to modify a *decision list* shown on the left side of Figure 5, which is a tree structure where branches extend in only one direction. Due to this asymmetric structure, the number of parameters does not increase exponentially with the depth, and the splitting order invariance does not exist. Moreover, subtree flip invariance also does not exist for any internal nodes except for the terminal splitting node, as shown in the left side of Figure 5. To completely remove this invariance, we virtually eliminate one of the terminal leaves by leaving the node empty, that is, a fixed prediction value of zero, as shown on the right side of Figure 5. Therefore only permutation invariance exists for our proposed architecture. We summarize invariances inherent to each model architecture in Table 1.

4 EXPERIMENT

We empirically evaluate barriers in soft tree ensembles to examine LMC.

4.1 SETUP

Datasets. In our experiments, we employed Tabular-Benchmark (Grinsztajn et al., 2022), a collection of tabular datasets suitable for evaluating tree ensembles. Details of datasets are provided in Section A in Appendix. As proposed in Grinsztajn et al. (2022), we randomly sampled $10,000$ instances for train and test data from each dataset. If the dataset contains fewer than $20,000$ instances, they are randomly divided into halves for train and test data. We applied quantile transformation to each feature and standardized it to follow a normal distribution.

Hyperparameters. We used three different learning rates $\eta \in \{0.01, 0.001, 0.0001\}$ and adopted the one that yields the highest training accuracy for each dataset. The batch size is set at 512. It is known that the optimal settings for the learning rate and batch size are interdependent (Smith et al., 2018). Therefore, it is reasonable to fix the batch size while adjusting the learning rate. During AM, we set the amount of data used for random sampling to be the same as the batch size, thus using 512 samples to measure the similarity of the tree outputs. As the number of trees M and their depths D vary for each experiment, these details will be specified in the experimental results section. During training, we minimized cross-entropy using Adam (Kingma & Ba, 2015) with its default hyperparameters[2]. Training is conducted for 50 epochs. To measure the barrier using Equation 1, experiments were conducted by interpolating between two models with $\lambda \in \{0, 1/24, \ldots, 23/24, 1\}$, which has the same granularity as in Ainsworth et al. (2023).

Randomness. We conducted experiments with five different random seed pairs: $r_A \in \{1, 3, 5, 7, 9\}$ and $r_B \in \{2, 4, 6, 8, 10\}$. As a result, the initial parameters and the contents of the data mini-batches during training are different in each training. In contrast to spawning (Frankle et al., 2020) that branches off from the exact same model partway through, we used more challenging practical conditions. The parameters $\boldsymbol{w}$, $\boldsymbol{b}$, and $\boldsymbol{\pi}$ were randomly initialized using a uniform distribution, identical to the procedure for a fully connected layer in the MLP[3].

[2] `https://pytorch.org/docs/stable/generated/torch.optim.Adam.html`
[3] `https://pytorch.org/docs/stable/generated/torch.nn.Linear.html`

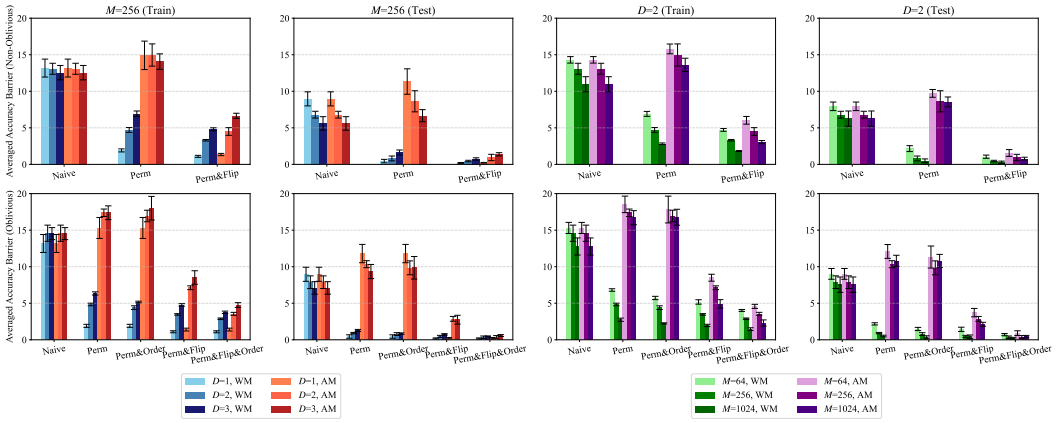

Figure 6: Barriers averaged across 16 datasets with respect to considered invariances for non-oblivious (top row) and oblivious (bottom row) trees. The error bars show the standard deviations of 5 executions.

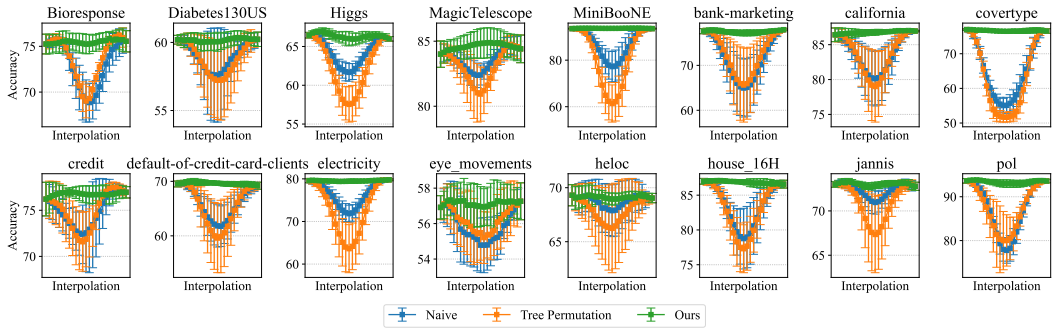

Figure 7: Interpolation curves of test accuracy for oblivious trees on 16 datasets from Tabular-Benchmark (Grinsztajn et al., 2022). Two model pairs are trained on the same dataset. The error bars show the standard deviations of 5 executions.

Resources. All experiments were conducted on a system equipped with an Intel Xeon E5-2698 CPU at 2.20 GHz, 252 GB of memory, and Tesla V100-DGXS-32GB GPU, running Ubuntu Linux (version 4.15.0-117-generic). The reproducible PyTorch (Paszke et al., 2019) implementation is provided in the supplementary material.

4.2 Results for Perfect Binary Trees

Figure 6 shows how the barrier between two perfect binary tree model pairs changes in each operation. The vertical axis of each plot in Figure 6 shows the averaged barrier over datasets for each considered invariance. The results for both the oblivious and non-oblivious trees are plotted separately in a vertical layout. The panels on the left display the results when the depth D of the tree varies, keeping $M = 256$ constant. The panels on the right show the results when the number of trees M varies, with D fixed at 2. For both oblivious and non-oblivious trees, we observed that the barrier significantly decreases as the considered invariances increase. Focusing on the test data results, after accounting for various invariances, the barrier is nearly zero, indicating that LMC has been achieved. In particular, the difference between the case of only permutation and the case where additional invariances are considered tends to be larger in the case of AM. This is because parameter values are not used during the rearrangement of the tree in AM. Additionally, it has been observed that the barrier increases as trees become deeper, and the barrier decreases as the number of trees increases. These behaviors correspond to the changes observed in neural networks when the depth varies or when the width of hidden layers increases (Entezari et al., 2022; Ainsworth et al., 2023). Figure 7 shows interpolation curves for AM in oblivious trees with $D = 2$ and $M = 256$. In our figures and tables, "Naive" refers to a straightforward parameter interpolation without any specific optimization; "Tree Permutation"

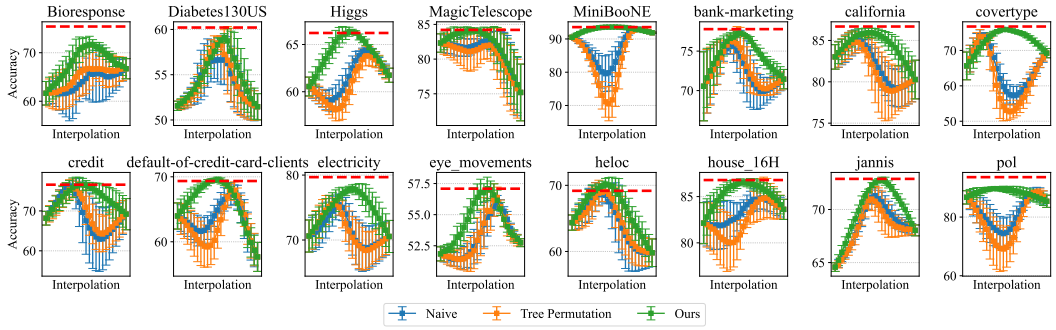

Figure 8: Interpolation curves of test accuracy for oblivious trees on 16 datasets from Tabular-Benchmark (Grinsztajn et al., 2022). Two model pairs are trained on split datasets with different class ratios. The error bars show the standard deviations of 5 executions. Performance of a model trained with the full dataset is shown in the red dashed horizontal lines as a reference.

or "Perm" considers only the permutation invariance; and "Ours" incorporates both the permutation of the trees and tree-inherent invariances. Other details, such as performance for each dataset, are provided in Section B in Appendix.

Furthermore, we conducted experiments with split data following the protocol in Ainsworth et al. (2023) and Jordan et al. (2023), where the initial split consists of randomly sampled 80% negative and 20% positive instances, and the second split inverts these ratios. There is no overlap between the two split datasets. We trained two model pairs using these separately split datasets and observed an improvement in performance by interpolating their parameters. Figure 8 illustrates the interpolation curves under AM in oblivious trees with parameters $D = 2$ and $M = 256$. Through model merging, it demonstrates similar performance to full data training even with split data training for the majority of datasets. Note that the data split is configured to remain consistent even when the training random seeds differ. Detailed results for each dataset using WM or AM are provided in Section B in Appendix.

Table 2 compares the average test barriers of an MLP with a ReLU activation function, whose width is equal to the number of trees, $M = 256$. The procedure for MLPs follows that described in Section 4.1. The permutation for MLPs is optimized using the method described in Ainsworth et al. (2023). Since Ainsworth et al. (2023) indicated that WM outperforms AM in neural networks, WM was used for the comparison. Overall, tree models exhibit smaller barriers compared to MLPs while keeping similar accuracy levels. It is important to note that MLPs with $D > 1$ tend to have more parameters at the same depth compared to trees, leading to more complex optimization landscapes. Nevertheless, the barrier for the non-oblivious tree at $D = 3$ is smaller than that for the MLP at $D = 2$, even with more parameters. Furthermore, at the same depth of $D = 1$, tree models have a smaller barrier. Here, the model size is evaluated using $F = 44$, the average input feature size of 16 datasets used in the experiments.

Table 2: Barriers, accuracies, and model sizes for MLP, non-oblivious trees, and oblivious trees.

Depth	MLP			
	Barrier		Accuracy	Size
	Naive	Perm		
1	8.755 ± 0.877	0.491 ± 0.062	76.286 ± 0.094	12034
2	15.341± 1.125	2.997 ± 0.709	75.981 ± 0.139	77826
3	15.915 ± 2.479	5.940 ± 2.153	75.935 ± 0.117	143618

Depth	Non-Oblivious Tree				
	Barrier			Accuracy	Size
	Naive	Perm	Ours		
1	8.965 ± 0.963	0.449 ± 0.235	0.181 ± 0.078	76.464 ± 0.167	12544
2	6.801 ± 0.464	0.811 ± 0.333	0.455 ± 0.105	76.631 ± 0.052	36608
3	5.602 ± 0.926	1.635 ± 0.334	0.740 ± 0.158	76.339 ± 0.115	84736

Depth	Oblivious Tree				
	Barrier			Accuracy	Size
	Naive	Perm	Ours		
1	8.965 ± 0.963	0.449 ± 0.235	0.181 ± 0.078	76.464 ± 0.167	12544
2	7.881 ± 0.866	0.918 ± 0.092	0.348 ± 0.172	76.623 ± 0.042	25088
3	7.096 ± 0.856	1.283 ± 0.139	0.484 ± 0.049	76.535 ± 0.063	38656

In Section 3.2, we have shown that considering additional invariances for deep perfect binary trees is computationally challenging, which may suggest developing heuristic algorithms for deep trees. However, we consider it is rather a low priority, supported by our observations that the barrier tends to increase as trees deepen even if we consider invariances. This trend indicates that deep models are fundamentally less important for model merging considerations. Furthermore, deep perfect binary trees are rarely used in practical scenarios. Kanoh & Sugiyama (2022) have demonstrated that generalization performance degrades with increasing depth in perfect binary trees due to the

Table 3: Barriers averaged for 16 datasets under WM with $D = 2$ and $M = 256$.

Architecture	Train				Test			
	Barrier			Accuracy	Barrier			Accuracy
	Naive	Perm	Ours		Naive	Perm	Ours	
Non-Oblivious Tree	13.079 ± 0.755	4.707 ± 0.332	3.303 ± 0.104	85.646 ± 0.090	6.801 ± 0.464	0.811 ± 0.333	0.455 ± 0.105	76.631 ± 0.052
Oblivious Tree	14.580 ± 1.108	4.834 ± 0.176	2.874 ± 0.108	85.808 ± 0.146	7.881 ± 0.866	0.919 ± 0.093	0.348 ± 0.172	76.623 ± 0.042
Decision List	13.835 ± 0.788	3.687 ± 0.230	—	85.337 ± 0.134	7.513 ± 0.944	0.436 ± 0.120	—	76.629 ± 0.119
Decision List (Modified)	12.922 ± 1.131	3.328 ± 0.204	—	85.563 ± 0.141	6.734 ± 1.096	0.468 ± 0.150	—	76.773 ± 0.051

Table 4: Barriers averaged for 16 datasets under AM with $D = 2$ and $M = 256$.

Architecture	Train				Test			
	Barrier			Accuracy	Barrier			Accuracy
	Naive	Perm	Ours		Naive	Perm	Ours	
Non-Oblivious Tree	13.079 ± 0.755	14.963 ± 1.520	4.500 ± 0.527	85.646 ± 0.090	6.801 ± 0.464	8.631 ± 1.444	0.943 ± 0.435	76.631 ± 0.052
Oblivious Tree	14.580 ± 1.108	17.380 ± 0.509	3.557 ± 0.201	85.808 ± 0.146	7.881 ± 0.866	10.349 ± 0.476	0.395 ± 0.185	76.623 ± 0.042
Decision List	13.835 ± 0.788	12.785 ± 1.924	—	85.337 ± 0.134	7.513 ± 0.944	7.452 ± 1.840	—	76.629 ± 0.119
Decision List (Modified)	12.922 ± 1.131	6.364 ± 0.194	—	85.563 ± 0.141	6.734 ± 1.096	2.114 ± 0.243	—	76.773 ± 0.051

degeneracy of the Neural Tangent Kernel (NTK) (Jacot et al., 2018). This evidence further supports the preference for shallow perfect binary trees, and increasing the number of trees can enhance the expressive power while reducing barriers.

4.3 Results for Decision Lists

We present empirical results of the original decision lists and our modified decision lists, as shown in Figure 5. As we have shown in Table 1, they have fewer invariances.

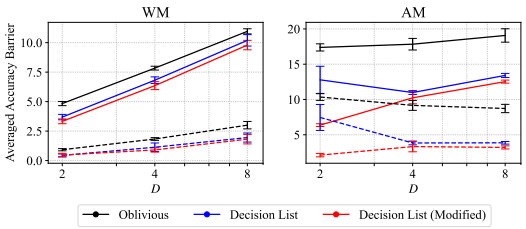

Figure 9: Averaged barrier for 16 datasets as a function of tree depth. The error bars show the standard deviations of 5 executions. The solid line represents the barrier in train accuracy, while the dashed line represents the barrier in test accuracy.

Figure 9 illustrates barriers as a function of depth, considering only permutation invariance, with M fixed at 256. In this experiment, we have excluded non-oblivious trees from comparison as the number of their parameters exponentially increases as trees deepen, making them infeasible computation. Our proposed modified decision lists reduce the barrier more effectively than both oblivious trees and the original decision lists. However, barriers of the modified decision lists are still larger than those obtained by considering additional invariances with perfect binary trees. Tables 3 and 4 show the averaged barriers for 16 datasets, with $D = 2$ and $M = 256$. Although barriers of modified decision lists are small when considering only permutations (Perm), perfect binary trees such as oblivious trees with additional invariances (Ours) exhibit smaller barriers, which supports the validity of using oblivious trees as in Popov et al. (2020) and Chang et al. (2022). To summarize, when considering the practical use of model merging, if the goal is to prioritize efficient computation, we recommend using our proposed decision list. Conversely, if the goal is to prioritize barriers, it would be preferable to use perfect binary trees, which have a greater number of invariances that maintain the functional behavior.

5 Conclusion

We have presented the first investigation of LMC for soft tree ensembles. We have identified additional invariances inherent in tree architectures and empirically demonstrated the importance of considering these factors. Achieving LMC is crucial not only for understanding the behavior of non-convex optimization from a learning theory perspective but also for implementing practical techniques such as model merging. By arithmetically combining parameters of differently trained models, a wide range of applications such as federated-leanning (McMahan et al., 2017) and continual-learning (Mirzadeh et al., 2021) have been explored. Our research extends these techniques to soft tree ensembles. We will leave these empirical investigations for future work.

ETHICS STATEMENT

This study provides a fundamental analysis of ensemble learning, and we believe that our discussion will not result in detrimental uses.

REPRODUCIBILITY STATEMENT

Source codes are available in the supplementary material to reproduce the numerical experiments and visualizations.

REFERENCES

Samuel Ainsworth, Jonathan Hayase, and Siddhartha Srinivasa. Git Re-Basin: Merging Models modulo Permutation Symmetries. In *International Conference on Learning Representations*, 2023.

Leo Breiman. Random Forests. In *Machine Learning*, 2001.

Chun-Hao Chang, Rich Caruana, and Anna Goldenberg. NODE-GAM: Neural generalized additive model for interpretable deep learning. In *International Conference on Learning Representations*, 2022.

An Mei Chen, Haw-minn Lu, and Robert Hecht-Nielsen. On the Geometry of Feedforward Neural Network Error Surfaces. *Neural Computation*, 1993.

David F. Crouse. On implementing 2D rectangular assignment algorithms. *IEEE Transactions on Aerospace and Electronic Systems*, 2016.

Rahim Entezari, Hanie Sedghi, Olga Saukh, and Behnam Neyshabur. The Role of Permutation Invariance in Linear Mode Connectivity of Neural Networks. In *International Conference on Learning Representations*, 2022.

Pierre Foret, Ariel Kleiner, Hossein Mobahi, and Behnam Neyshabur. Sharpness-aware Minimization for Efficiently Improving Generalization. In *International Conference on Learning Representations*, 2021.

Jonathan Frankle, Gintare Karolina Dziugaite, Daniel Roy, and Michael Carbin. Linear Mode Connectivity and the Lottery Ticket Hypothesis. In *Proceedings of the 37th International Conference on Machine Learning*, 2020.

Nicholas Frosst and Geoffrey E. Hinton. Distilling a Neural Network Into a Soft Decision Tree. *CoRR*, 2017.

Leo Grinsztajn, Edouard Oyallon, and Gael Varoquaux. Why do tree-based models still outperform deep learning on typical tabular data? In *Thirty-sixth Conference on Neural Information Processing Systems Datasets and Benchmarks Track*, 2022.

Fidel A. Guerrero Peña, Heitor Rapela Medeiros, Thomas Dubail, Masih Aminbeidokhti, Eric Granger, and Marco Pedersoli. Re-basin via implicit Sinkhorn differentiation. In *IEEE/CVF Conference on Computer Vision and Pattern Recognition*, 2023.

Hussein Hazimeh, Natalia Ponomareva, Petros Mol, Zhenyu Tan, and Rahul Mazumder. The Tree Ensemble Layer: Differentiability meets Conditional Computation. In *Proceedings of the 37th International Conference on Machine Learning*, 2020.

Robert Hecht-Nielsen. On the algebraic structure of feedforward network weight spaces. In *Advanced Neural Computers*. 1990.

Arthur Jacot, Franck Gabriel, and Clement Hongler. Neural Tangent Kernel: Convergence and Generalization in Neural Networks. In *Advances in Neural Information Processing Systems*, 2018.

Albert Q. Jiang, Alexandre Sablayrolles, Antoine Roux, Arthur Mensch, Blanche Savary, Chris Bamford, Devendra Singh Chaplot, Diego de las Casas, Emma Bou Hanna, Florian Bressand, Gianna Lengyel, Guillaume Bour, Guillaume Lample, Lélio Renard Lavaud, Lucile Saulnier, Marie-Anne Lachaux, Pierre Stock, Sandeep Subramanian, Sophia Yang, Szymon Antoniak, Teven Le Scao, Théophile Gervet, Thibaut Lavril, Thomas Wang, Timothée Lacroix, and William El Sayed. Mixtral of experts, 2024.

Keller Jordan, Hanie Sedghi, Olga Saukh, Rahim Entezari, and Behnam Neyshabur. REPAIR: REnormalizing permuted activations for interpolation repair. In *International Conference on Learning Representations*, 2023.

M.I. Jordan and R.A. Jacobs. Hierarchical mixtures of experts and the EM algorithm. In *Proceedings of International Conference on Neural Networks*, 1993.

Ryuichi Kanoh and Mahito Sugiyama. A Neural Tangent Kernel Perspective of Infinite Tree Ensembles. In *International Conference on Learning Representations*, 2022.

Ryuichi Kanoh and Mahito Sugiyama. Analyzing Tree Architectures in Ensembles via Neural Tangent Kernel. In *International Conference on Learning Representations*, 2023.

Guolin Ke, Zhenhui Xu, Jia Zhang, Jiang Bian, and Tie-Yan Liu. DeepGBM: A Deep Learning Framework Distilled by GBDT for Online Prediction Tasks. In *Proceedings of the 25th ACM SIGKDD International Conference on Knowledge Discovery & Data Mining*, 2019.

Diederik Kingma and Jimmy Ba. Adam: A Method for Stochastic Optimization. In *International Conference on Learning Representations*, 2015.

Yann LeCun and Corinna Cortes. MNIST handwritten digit database. 2010.

Dmitry Lepikhin, HyoukJoong Lee, Yuanzhong Xu, Dehao Chen, Orhan Firat, Yanping Huang, Maxim Krikun, Noam Shazeer, and Zhifeng Chen. GShard: Scaling Giant Models with Conditional Computation and Automatic Sharding. In *International Conference on Learning Representations*, 2021.

Brendan McMahan, Eider Moore, Daniel Ramage, Seth Hampson, and Blaise Aguera y Arcas. Communication-Efficient Learning of Deep Networks from Decentralized Data. In *Proceedings of the 20th International Conference on Artificial Intelligence and Statistics*, 2017.

Seyed Iman Mirzadeh, Mehrdad Farajtabar, Dilan Gorur, Razvan Pascanu, and Hassan Ghasemzadeh. Linear Mode Connectivity in Multitask and Continual Learning. In *International Conference on Learning Representations*, 2021.

Sreerama K. Murthy, Simon Kasif, and Steven Salzberg. A system for induction of oblique decision trees. *Journal of Artificial Intelligence Research*, 1994.

Guillermo Ortiz-Jimenez, Alessandro Favero, and Pascal Frossard. Task Arithmetic in the Tangent Space: Improved Editing of Pre-Trained Models. In *Thirty-seventh Conference on Neural Information Processing Systems*, 2023.

Adam Paszke, Sam Gross, Francisco Massa, Adam Lerer, James Bradbury, Gregory Chanan, Trevor Killeen, Zeming Lin, Natalia Gimelshein, Luca Antiga, Alban Desmaison, Andreas Kopf, Edward Yang, Zachary DeVito, Martin Raison, Alykhan Tejani, Sasank Chilamkurthy, Benoit Steiner, Lu Fang, Junjie Bai, and Soumith Chintala. PyTorch: An Imperative Style, High-Performance Deep Learning Library. In *Advances in Neural Information Processing Systems*, 2019.

Sergei Popov, Stanislav Morozov, and Artem Babenko. Neural Oblivious Decision Ensembles for Deep Learning on Tabular Data. In *International Conference on Learning Representations*, 2020.

Byron Roe. MiniBooNE particle identification. UCI Machine Learning Repository, 2010.

Noam Shazeer, Azalia Mirhoseini, Krzysztof Maziarz, Andy Davis, Quoc V. Le, Geoffrey E. Hinton, and Jeff Dean. Outrageously Large Neural Networks: The Sparsely-Gated Mixture-of-Experts Layer. In *International Conference on Learning Representations*, 2017.

Samuel L. Smith, Pieter-Jan Kindermans, and Quoc V. Le. Don't Decay the Learning Rate, Increase the Batch Size. In *International Conference on Learning Representations*, 2018.

Nitish Srivastava, Geoffrey Hinton, Alex Krizhevsky, Ilya Sutskever, and Ruslan Salakhutdinov. Dropout: A Simple Way to Prevent Neural Networks from Overfitting. *Journal of Machine Learning Research*, 2014.

Mitchell Wortsman, Gabriel Ilharco, Samir Ya Gadre, Rebecca Roelofs, Raphael Gontijo-Lopes, Ari S Morcos, Hongseok Namkoong, Ali Farhadi, Yair Carmon, Simon Kornblith, and Ludwig Schmidt. Model soups: averaging weights of multiple fine-tuned models improves accuracy without increasing inference time. In *Proceedings of the 39th International Conference on Machine Learning*, 2022.

Prateek Yadav, Derek Tam, Leshem Choshen, Colin Raffel, and Mohit Bansal. TIES-merging: Resolving interference when merging models. In *Thirty-seventh Conference on Neural Information Processing Systems*, 2023.

Zhanpeng Zhou, Yongyi Yang, Xiaojiang Yang, Junchi Yan, and Wei Hu. Going Beyond Linear Mode Connectivity: The Layerwise Linear Feature Connectivity. In *Thirty-seventh Conference on Neural Information Processing Systems*, 2023.

A DATASET

Details of datasets used in experiments are provided in Table 5.

Table 5: Summary of the datasets used in the experiments.

Dataset	N	F	**Link**
Bioresponse	3434	419	https://www.openml.org/d/45019
Diabetes130US	71090	7	https://www.openml.org/d/45022
Higgs	940160	24	https://www.openml.org/d/44129
MagicTelescope	13376	10	https://www.openml.org/d/44125
MiniBooNE	72998	50	https://www.openml.org/d/44128
bank-marketing	10578	7	https://www.openml.org/d/44126
california	20634	8	https://www.openml.org/d/45028
covertype	566602	10	https://www.openml.org/d/44121
credit	16714	10	https://www.openml.org/d/44089
default-of-credit-card-clients	13272	20	https://www.openml.org/d/45020
electricity	38474	7	https://www.openml.org/d/44120
eye_movements	7608	20	https://www.openml.org/d/44130
heloc	10000	22	https://www.openml.org/d/45026
house_16H	13488	16	https://www.openml.org/d/44123
jannis	57580	54	https://www.openml.org/d/45021
pol	10082	26	https://www.openml.org/d/44122

B ADDITIONAL EMPIRICAL RESULTS

Tables 6, 7, 8 and 9 present the barrier for each dataset with $D = 2$ and $M = 256$. By incorporating additional invariances, it has been possible to consistently reduce the barriers.

Tables 10 and 11 detail the characteristics of the barriers in the decision lists for each dataset with $D = 2$ and $M = 256$. The barriers in the modified decision lists tend to be smaller.

Tables 12 and 13 show the barrier for each model when only considering permutations with $D = 2$ and $M = 256$. It is evident that focusing solely on permutations leads to smaller barriers in the modified decision lists compared to other architectures.

Figures 10, 11, 12, 13, 14, 15, 16 and 17 show the interpolation curves of oblivious trees with $D = 2$ and $M = 256$ across various datasets and configurations. Significant improvements are particularly noticeable in AM, but improvements are also observed in WM. These characteristics are also apparent in the non-oblivious trees, as shown in Figures 18, 19, 20, 21, 22, 23, 24 and 25. Regarding split data training, the dataset for each of the two classes is initially complete (100%). It is then divided into splits of 80% and 20%, and 20% and 80%, respectively. Each model is trained using these splits. Figures 14, 16, 22, and 24 show the training accuracy evaluated using the full dataset (100% for each class). In split data training, the performance reference of full data training is shown only for the performance on the test data. This is because, in split data training, even the training dataset used for evaluation includes portions that are not used for training each model, which differs from the conditions in full data training. In contrast, when evaluating performance on the test data, all of the test data has not been used equally for the training of each model, which allows for a fair comparison between the two approaches. Figures 26, 27, 28, 29, 30, 31, 32, 33, 34, 35, 36, 37, 38, 39, 40 and 41 visualize the same to that of perfect binary trees for the decision lists.

Figures 42 and 43 show the interpolation curves for MNIST (LeCun & Cortes, 2010) with various tree architectures where $D = 2$ and $M = 256$. Although MNIST consists of 2-dimensional image data, it is input as a 1-dimensional vector.

Table 6: Accuracy barrier for non-oblivious trees with WM.

Dataset	Train			Test		
	Naive	**Perm**	**Perm&Flip**	**Naive**	**Perm**	**Perm&Flip**
Bioresponse	18.944 ± 10.076	5.876 ± 1.477	4.132 ± 0.893	8.235 ± 6.456	1.285 ± 0.635	0.314 ± 0.432
Diabetes130US	2.148 ± 0.601	1.388 ± 1.159	0.947 ± 0.888	1.014 ± 0.959	0.540 ± 0.999	0.784 ± 0.840
Higgs	27.578 ± 1.742	18.470 ± 0.769	14.772 ± 1.419	4.055 ± 1.089	0.662 ± 0.590	0.292 ± 0.421
MagicTelescope	2.995 ± 1.198	0.576 ± 0.556	0.307 ± 0.346	2.096 ± 1.055	0.361 ± 0.618	0.229 ± 0.348
MiniBooNE	18.238 ± 4.570	2.272 ± 0.215	1.506 ± 0.211	12.592 ± 4.190	0.231 ± 0.314	0.000 ± 0.000
bank-marketing	13.999 ± 4.110	2.711 ± 1.183	1.521 ± 0.463	13.593 ± 4.567	1.843 ± 1.001	0.953 ± 0.688
california	6.396 ± 2.472	0.873 ± 0.551	0.520 ± 0.327	5.226 ± 2.377	0.224 ± 0.248	0.206 ± 0.131
covertype	16.823 ± 4.159	1.839 ± 0.336	0.914 ± 0.546	14.900 ± 4.016	1.035 ± 0.106	0.376 ± 0.333
credit	7.317 ± 2.425	3.172 ± 2.636	2.615 ± 0.831	5.861 ± 2.064	2.202 ± 3.103	1.830 ± 0.588
default-of-credit-card-clients	14.318 ± 4.509	5.419 ± 1.318	3.273 ± 0.793	6.227 ± 4.205	0.937 ± 1.036	0.243 ± 0.172
electricity	10.090 ± 2.930	1.035 ± 0.543	0.221 ± 0.192	9.422 ± 2.795	0.771 ± 0.478	0.130 ± 0.071
eye_movements	18.743 ± 1.994	11.605 ± 1.927	7.866 ± 1.301	1.495 ± 0.467	0.463 ± 0.183	0.180 ± 0.206
heloc	4.434 ± 1.611	1.652 ± 0.475	1.012 ± 0.481	0.830 ± 0.727	0.475 ± 0.447	0.322 ± 0.338
house_16H	8.935 ± 2.504	3.362 ± 0.482	2.660 ± 1.208	4.230 ± 2.189	0.219 ± 0.224	0.404 ± 0.782
jannis	17.756 ± 3.322	10.442 ± 1.404	7.362 ± 0.219	3.205 ± 2.849	0.029 ± 0.064	0.007 ± 0.016
pol	20.542 ± 2.873	4.612 ± 0.912	3.225 ± 1.080	15.830 ± 2.562	1.708 ± 0.599	1.012 ± 0.859

Table 7: Accuracy barrier for non-oblivious trees with AM.

Dataset	Train			Test		
	Naive	**Perm**	**Perm&Flip**	**Naive**	**Perm**	**Perm&Flip**
Bioresponse	18.944 ± 10.076	14.066 ± 7.045	5.710 ± 0.915	8.235 ± 6.456	5.037 ± 3.141	0.966 ± 0.316
Diabetes130US	2.148 ± 0.601	3.086 ± 2.566	0.574 ± 0.365	1.014 ± 0.959	1.936 ± 2.878	0.105 ± 0.152
Higgs	27.578 ± 1.742	30.704 ± 2.899	18.435 ± 1.599	4.055 ± 1.089	7.272 ± 1.089	1.044 ± 0.483
MagicTelescope	2.995 ± 1.198	3.309 ± 1.486	0.778 ± 0.515	2.096 ± 1.055	2.693 ± 1.190	0.428 ± 0.327
MiniBooNE	18.238 ± 4.570	34.934 ± 8.157	2.332 ± 0.383	12.592 ± 4.190	28.721 ± 7.869	0.074 ± 0.081
bank-marketing	13.999 ± 4.110	13.598 ± 7.638	3.098 ± 0.539	13.593 ± 4.567	12.810 ± 7.605	2.643 ± 0.704
california	6.396 ± 2.472	5.800 ± 2.036	0.697 ± 0.535	5.226 ± 2.377	4.858 ± 2.017	0.261 ± 0.285
covertype	16.823 ± 4.159	19.708 ± 6.392	1.420 ± 0.619	14.900 ± 4.016	17.765 ± 6.400	0.758 ± 0.540
credit	7.317 ± 2.425	10.556 ± 8.753	3.640 ± 1.624	5.861 ± 2.064	9.378 ± 9.083	2.551 ± 1.987
default-of-credit-card-clients	14.318 ± 4.509	14.166 ± 2.297	4.247 ± 1.678	6.227 ± 4.205	6.514 ± 2.049	0.885 ± 1.852
electricity	10.090 ± 2.930	12.955 ± 4.558	0.762 ± 0.332	9.422 ± 2.795	12.261 ± 4.554	0.499 ± 0.260
eye_movements	18.743 ± 1.994	18.757 ± 1.273	10.957 ± 1.019	1.495 ± 0.467	1.583 ± 1.011	0.146 ± 0.167
heloc	4.434 ± 1.611	6.564 ± 2.404	1.774 ± 0.672	0.830 ± 0.727	2.179 ± 2.100	0.385 ± 0.370
house_16H	8.935 ± 2.504	10.184 ± 2.667	3.908 ± 0.863	4.230 ± 2.189	5.664 ± 2.461	1.056 ± 0.693
jannis	17.756 ± 3.322	19.004 ± 1.246	9.890 ± 1.036	3.205 ± 2.849	4.047 ± 1.415	0.346 ± 0.443
pol	20.542 ± 2.873	16.267 ± 3.914	7.967 ± 3.208	15.830 ± 2.562	12.863 ± 3.983	4.539 ± 2.727

Table 8: Accuracy barrier for oblivious trees with WM.

Dataset	Train			Test		
	Naive	**Perm**	**Perm&Order&Flip**	**Naive**	**Perm**	**Perm&Order&Flip**
Bioresponse	16.642 ± 4.362	4.800 ± 0.895	3.289 ± 0.680	7.165 ± 2.547	1.069 ± 1.020	0.299 ± 0.247
Diabetes130US	3.170 ± 3.304	1.120 ± 1.123	0.246 ± 0.177	2.831 ± 3.476	0.882 ± 1.309	0.181 ± 0.155
Higgs	28.640 ± 0.914	19.754 ± 1.023	13.689 ± 0.814	4.648 ± 0.966	1.270 ± 0.808	0.266 ± 0.232
MagicTelescope	2.659 ± 1.637	0.473 ± 0.632	0.077 ± 0.110	2.012 ± 1.343	0.534 ± 0.565	0.093 ± 0.144
MiniBooNE	22.344 ± 7.001	2.388 ± 0.194	1.628 ± 0.208	16.454 ± 6.706	0.075 ± 0.086	0.012 ± 0.019
bank-marketing	13.512 ± 6.416	2.998 ± 1.582	0.925 ± 0.688	12.856 ± 6.609	2.324 ± 1.618	0.634 ± 0.433
california	8.281 ± 4.253	0.874 ± 0.524	0.351 ± 0.267	6.578 ± 4.264	0.342 ± 0.209	0.034 ± 0.024
covertype	23.977 ± 2.565	2.073 ± 0.657	0.976 ± 0.523	21.790 ± 2.253	0.992 ± 0.496	0.422 ± 0.319
credit	6.912 ± 4.083	2.369 ± 0.887	0.662 ± 0.606	5.739 ± 4.502	1.324 ± 0.674	0.350 ± 0.522
default-of-credit-card-clients	16.301 ± 4.462	4.512 ± 1.033	2.902 ± 0.620	7.618 ± 3.873	0.728 ± 0.331	0.531 ± 0.557
electricity	8.835 ± 1.824	1.060 ± 0.684	0.279 ± 0.266	7.952 ± 1.995	0.731 ± 0.383	0.285 ± 0.200
eye_movements	22.604 ± 1.486	12.687 ± 1.645	7.826 ± 1.822	2.884 ± 1.646	0.825 ± 0.711	0.607 ± 0.259
heloc	6.282 ± 2.351	2.517 ± 1.156	1.507 ± 0.498	1.625 ± 1.480	0.869 ± 0.957	0.727 ± 0.785
house_16H	13.600 ± 5.135	3.302 ± 0.376	1.950 ± 0.346	8.055 ± 4.429	0.330 ± 0.441	0.158 ± 0.098
jannis	19.390 ± 1.013	11.358 ± 0.377	7.140 ± 0.538	1.999 ± 1.237	0.305 ± 0.409	0.214 ± 0.235
pol	20.125 ± 2.902	5.059 ± 1.482	2.544 ± 1.005	15.887 ± 3.061	2.100 ± 1.358	0.751 ± 0.892

Table 9: Accuracy barrier for oblivious trees with AM.

Dataset	Train			Test		
	Naive	**Perm**	**Perm&Order&Flip**	**Naive**	**Perm**	**Perm&Order&Flip**
Bioresponse	16.642 ± 4.362	19.033 ± 8.533	6.358 ± 1.915	7.165 ± 2.547	6.904 ± 5.380	1.038 ± 0.591
Diabetes130US	3.170 ± 3.304	5.473 ± 3.260	0.703 ± 0.517	2.831 ± 3.476	5.290 ± 3.486	0.390 ± 0.291
Higgs	28.640 ± 0.914	33.234 ± 3.164	15.678 ± 0.713	4.648 ± 0.966	8.113 ± 2.614	0.415 ± 0.454
MagicTelescope	2.659 ± 1.637	3.902 ± 1.931	0.224 ± 0.256	2.012 ± 1.343	3.687 ± 1.876	0.334 ± 0.434
MiniBooNE	22.344 ± 7.001	41.022 ± 3.398	2.184 ± 0.425	16.454 ± 6.706	34.452 ± 3.161	0.033 ± 0.056
bank-marketing	13.512 ± 6.416	12.248 ± 6.748	1.330 ± 0.806	12.856 ± 6.609	11.356 ± 7.168	0.695 ± 0.464
california	8.281 ± 4.253	9.539 ± 4.798	0.371 ± 0.365	6.578 ± 4.264	8.354 ± 4.648	0.112 ± 0.181
covertype	23.977 ± 2.565	27.590 ± 2.172	1.051 ± 0.407	21.790 ± 2.253	25.289 ± 1.787	0.403 ± 0.236
credit	6.912 ± 4.083	9.839 ± 6.698	1.169 ± 0.839	5.739 ± 4.502	8.291 ± 7.268	0.549 ± 0.751
default-of-credit-card-clients	16.301 ± 4.462	21.746 ± 7.075	3.646 ± 0.520	7.618 ± 3.873	12.183 ± 5.954	0.285 ± 0.372
electricity	8.835 ± 1.824	18.177 ± 5.979	0.472 ± 0.507	7.952 ± 1.995	17.396 ± 5.809	0.405 ± 0.356
eye_movements	22.604 ± 1.486	23.221 ± 3.024	8.588 ± 2.248	2.884 ± 1.646	2.761 ± 1.628	0.398 ± 0.435
heloc	6.282 ± 2.351	9.074 ± 3.894	2.541 ± 0.471	1.625 ± 1.480	3.891 ± 2.655	0.485 ± 0.397
house_16H	13.600 ± 5.135	17.963 ± 5.099	2.841 ± 0.543	8.055 ± 4.429	12.192 ± 4.635	0.292 ± 0.157
jannis	19.390 ± 1.013	22.482 ± 3.113	9.570 ± 0.316	1.999 ± 1.237	4.292 ± 2.509	0.069 ± 0.154
pol	20.125 ± 2.902	19.558 ± 5.785	3.056 ± 0.510	15.887 ± 3.061	14.858 ± 5.523	0.961 ± 0.722

Table 10: Accuracy barrier for decision lists with WM.

Dataset	Train				Test			
	Naive	Perm	Naive (Modified)	Perm (Modified)	Naive	Perm	Naive (Modified)	Perm (Modified)
Bioresponse	21.323 ± 6.563	4.259 ± 0.698	14.578 ± 3.930	4.641 ± 0.918	9.325 ± 3.988	0.346 ± 0.277	7.346 ± 4.261	1.309 ± 0.827
Diabetes130US	5.182 ± 3.745	1.483 ± 1.006	2.754 ± 1.098	1.088 ± 0.608	4.910 ± 4.244	1.293 ± 1.332	1.476 ± 1.308	0.849 ± 0.885
Higgs	27.778 ± 1.036	16.110 ± 0.518	28.915 ± 1.314	14.071 ± 0.395	4.777 ± 0.803	0.106 ± 0.203	5.136 ± 0.946	0.039 ± 0.083
MagicTelescope	4.855 ± 3.388	0.355 ± 0.682	5.138 ± 2.655	0.182 ± 0.141	4.137 ± 3.763	0.280 ± 0.519	4.534 ± 2.588	0.157 ± 0.162
MiniBooNE	23.059 ± 1.479	1.911 ± 0.138	14.916 ± 3.616	1.580 ± 0.178	17.248 ± 1.683	0.025 ± 0.036	9.340 ± 3.585	0.035 ± 0.042
bank-marketing	11.952 ± 3.794	0.979 ± 0.478	11.589 ± 2.167	0.373 ± 0.448	11.387 ± 4.113	0.536 ± 0.472	10.540 ± 2.067	0.349 ± 0.348
california	6.522 ± 3.195	0.621 ± 0.363	8.435 ± 3.273	0.538 ± 0.214	5.167 ± 2.962	0.236 ± 0.146	6.844 ± 3.087	0.151 ± 0.147
covertype	13.408 ± 3.839	1.341 ± 0.433	11.114 ± 2.689	1.257 ± 0.904	11.162 ± 3.620	0.472 ± 0.340	8.826 ± 2.729	0.477 ± 0.889
credit	11.238 ± 8.115	1.968 ± 0.990	14.626 ± 5.448	1.390 ± 0.423	10.880 ± 9.040	1.421 ± 1.046	13.667 ± 5.951	0.940 ± 0.612
default-of-credit-card-clients	12.513 ± 5.116	3.107 ± 1.123	11.378 ± 2.123	3.793 ± 0.881	5.161 ± 4.304	0.328 ± 0.512	3.197 ± 1.916	0.666 ± 0.651
electricity	6.524 ± 1.863	0.725 ± 0.451	9.101 ± 2.685	0.944 ± 0.557	5.834 ± 1.838	0.420 ± 0.354	8.487 ± 2.460	0.543 ± 0.511
eye_movements	19.125 ± 1.791	9.433 ± 1.385	19.738 ± 1.490	8.755 ± 1.391	1.990 ± 1.623	0.329 ± 0.102	1.916 ± 1.492	0.277 ± 0.302
heloc	4.513 ± 1.826	1.564 ± 0.617	5.116 ± 0.793	1.574 ± 0.154	0.725 ± 0.598	0.155 ± 0.190	1.263 ± 0.711	0.359 ± 0.346
house_16H	9.195 ± 2.408	2.520 ± 0.446	8.693 ± 1.302	2.222 ± 0.730	4.629 ± 2.314	0.063 ± 0.129	4.192 ± 1.517	0.185 ± 0.296
jannis	20.766 ± 2.097	9.484 ± 0.371	20.520 ± 1.017	7.400 ± 0.324	3.947 ± 2.605	0.006 ± 0.013	4.451 ± 1.300	0.004 ± 0.009
pol	23.401 ± 5.448	3.137 ± 1.038	20.137 ± 4.200	3.435 ± 0.675	18.933 ± 5.249	0.952 ± 0.925	16.522 ± 3.502	1.143 ± 0.565

Table 11: Accuracy barrier for decision lists with AM.

Dataset	Train				Test			
	Naive	Perm	Naive (Modified)	Perm (Modified)	Naive	Perm	Naive (Modified)	Perm (Modified)
Bioresponse	21.323 ± 6.563	13.349 ± 5.943	14.578 ± 3.930	10.363 ± 7.256	9.325 ± 3.988	4.817 ± 2.825	7.346 ± 4.261	3.871 ± 4.608
Diabetes130US	5.182 ± 3.745	5.590 ± 3.328	2.754 ± 1.098	1.371 ± 0.507	4.910 ± 4.244	4.926 ± 3.796	1.476 ± 1.308	0.694 ± 0.649
Higgs	27.778 ± 1.036	28.910 ± 2.132	28.915 ± 1.314	20.131 ± 1.693	4.777 ± 0.803	6.722 ± 1.231	5.136 ± 0.946	1.755 ± 1.403
MagicTelescope	4.855 ± 3.388	3.349 ± 3.273	5.138 ± 2.655	1.451 ± 0.705	4.137 ± 3.763	3.001 ± 3.478	4.534 ± 2.588	1.090 ± 0.437
MiniBooNE	23.059 ± 1.479	18.149 ± 7.500	14.916 ± 3.616	3.870 ± 1.168	17.248 ± 1.683	13.868 ± 7.222	9.340 ± 3.585	0.797 ± 0.860
bank-marketing	11.952 ± 3.794	9.782 ± 6.722	11.589 ± 2.167	2.815 ± 0.957	11.387 ± 4.113	9.151 ± 7.204	10.540 ± 2.067	2.521 ± 1.055
california	6.522 ± 3.195	5.812 ± 2.365	8.435 ± 3.273	2.254 ± 0.813	5.167 ± 2.962	4.899 ± 2.018	6.844 ± 3.087	1.186 ± 0.643
covertype	13.408 ± 3.839	14.727 ± 7.029	11.114 ± 2.689	4.036 ± 1.450	11.162 ± 3.620	13.352 ± 7.056	8.826 ± 2.729	2.656 ± 1.302
credit	11.238 ± 8.115	18.620 ± 9.806	14.626 ± 5.448	8.979 ± 6.919	10.880 ± 9.040	18.606 ± 10.015	13.667 ± 5.951	8.113 ± 6.633
default-of-credit-card-clients	12.513 ± 5.116	12.880 ± 5.070	11.378 ± 2.123	6.055 ± 1.178	5.161 ± 4.304	6.465 ± 5.062	3.197 ± 1.916	0.533 ± 0.239
electricity	6.524 ± 1.863	4.988 ± 2.732	9.101 ± 2.685	3.041 ± 0.676	5.834 ± 1.838	4.361 ± 2.532	8.487 ± 2.460	2.637 ± 0.730
eye_movements	19.125 ± 1.791	18.694 ± 1.774	19.738 ± 1.490	13.408 ± 1.196	1.990 ± 1.623	3.046 ± 1.625	1.916 ± 1.492	1.807 ± 1.312
heloc	4.513 ± 1.826	5.504 ± 1.650	5.116 ± 0.793	3.287 ± 0.758	0.725 ± 0.598	1.711 ± 1.278	1.263 ± 0.711	0.528 ± 0.147
house_16H	9.195 ± 2.408	8.591 ± 3.370	8.693 ± 1.302	3.937 ± 0.816	4.629 ± 2.314	4.547 ± 2.726	4.192 ± 1.517	0.751 ± 0.508
jannis	20.766 ± 2.097	20.768 ± 2.200	20.520 ± 1.017	12.008 ± 0.892	3.947 ± 2.605	6.472 ± 2.342	4.451 ± 1.300	0.106 ± 0.162
pol	23.401 ± 5.448	17.384 ± 6.441	20.137 ± 4.200	10.339 ± 2.743	18.933 ± 5.249	13.285 ± 5.863	16.522 ± 3.502	6.492 ± 2.536

Table 12: Training accuracy barrier for permuted models with WM. The numbers in parentheses represent the original accuracy.

Dataset	Non-Oblivious Tree	Oblivious Tree	Decision List	Decision List (Modified)
Bioresponse	5.876 ± 1.477 (93.005)	4.800 ± 0.895 (91.753)	4.259 ± 0.698 (91.771)	4.641 ± 0.918 (90.489)
Diabetes130US	1.388 ± 1.159 (60.686)	1.120 ± 1.123 (60.567)	1.483 ± 1.006 (60.425)	1.088 ± 0.608 (61.178)
Higgs	18.470 ± 0.769 (97.232)	19.754 ± 1.023 (97.616)	16.110 ± 0.518 (95.838)	14.071 ± 0.395 (95.831)
MagicTelescope	0.576 ± 0.556 (84.963)	0.473 ± 0.632 (84.460)	0.355 ± 0.682 (84.999)	0.182 ± 0.141 (85.411)
MiniBooNE	2.272 ± 0.215 (99.980)	2.388 ± 0.194 (99.980)	1.911 ± 0.138 (99.977)	1.580 ± 0.178 (99.976)
bank-marketing	2.711 ± 1.183 (79.490)	2.998 ± 1.582 (79.351)	0.979 ± 0.478 (79.166)	0.373 ± 0.448 (79.709)
california	0.873 ± 0.551 (87.897)	0.874 ± 0.524 (87.909)	0.621 ± 0.363 (88.012)	0.538 ± 0.214 (88.054)
covertype	1.839 ± 0.336 (79.445)	2.073 ± 0.657 (79.754)	1.341 ± 0.433 (79.618)	1.257 ± 0.904 (79.550)
credit	3.172 ± 2.636 (78.679)	2.369 ± 0.887 (78.231)	1.968 ± 0.990 (78.166)	1.390 ± 0.423 (78.905)
default-of-credit-card-clients	5.419 ± 1.318 (78.017)	4.512 ± 1.033 (78.657)	3.107 ± 1.123 (77.315)	3.793 ± 0.881 (78.308)
electricity	1.035 ± 0.543 (80.375)	1.060 ± 0.684 (80.861)	0.725 ± 0.451 (80.396)	0.944 ± 0.557 (80.651)
eye_movements	11.605 ± 1.927 (81.693)	12.687 ± 1.645 (83.730)	9.433 ± 1.385 (81.075)	8.755 ± 1.391 (81.451)
heloc	1.652 ± 0.475 (77.430)	2.517 ± 1.156 (78.370)	1.564 ± 0.617 (77.968)	1.574 ± 0.154 (78.550)
house_16H	3.362 ± 0.482 (93.093)	3.302 ± 0.376 (93.351)	2.520 ± 0.446 (92.783)	2.222 ± 0.730 (93.058)
jannis	10.442 ± 1.404 (100.000)	11.358 ± 0.377 (100.000)	9.484 ± 0.371 (100.000)	7.400 ± 0.324 (100.000)
pol	4.612 ± 0.912 (98.348)	5.059 ± 1.482 (98.340)	3.137 ± 1.038 (97.883)	3.435 ± 0.675 (97.881)

Table 13: Training accuracy barrier for permuted models with AM. The numbers in parentheses represent the original accuracy.

Dataset	Non-Oblivious	Oblivious	Decision List	Decision List (Modified)
Bioresponse	14.066 ± 7.045 (93.005)	19.033 ± 8.533 (91.753)	13.349 ± 5.943 (91.771)	10.363 ± 7.256 (90.489)
Diabetes130US	3.086 ± 2.566 (60.686)	5.473 ± 3.260 (60.567)	5.590 ± 3.328 (60.425)	1.371 ± 0.507 (61.178)
Higgs	30.704 ± 2.899 (97.232)	33.234 ± 3.164 (97.616)	28.910 ± 2.132 (95.838)	20.131 ± 1.693 (95.831)
MagicTelescope	3.309 ± 1.486 (84.963)	3.902 ± 1.931 (84.460)	3.349 ± 3.273 (84.999)	1.451 ± 0.705 (85.411)
MiniBooNE	34.934 ± 8.157 (99.980)	41.022 ± 3.398 (99.980)	18.149 ± 7.500 (99.977)	3.870 ± 1.168 (99.976)
bank-marketing	13.598 ± 7.638 (79.490)	12.248 ± 6.748 (79.351)	9.782 ± 6.722 (79.166)	2.815 ± 0.957 (79.709)
california	5.800 ± 2.036 (87.897)	9.539 ± 4.798 (87.909)	5.812 ± 2.365 (88.012)	2.254 ± 0.813 (88.054)
covertype	19.708 ± 6.392 (79.445)	27.590 ± 2.172 (79.754)	14.727 ± 7.029 (79.618)	4.036 ± 1.450 (79.550)
credit	10.556 ± 8.753 (78.679)	9.839 ± 6.698 (78.231)	18.620 ± 9.806 (78.166)	8.979 ± 6.919 (78.905)
default-of-credit-card-clients	14.166 ± 2.297 (78.017)	21.746 ± 7.075 (78.657)	12.880 ± 5.070 (77.315)	6.055 ± 1.178 (78.308)
electricity	12.955 ± 4.558 (80.375)	18.177 ± 5.979 (80.861)	4.988 ± 2.732 (80.396)	3.041 ± 0.676 (80.651)
eye_movements	18.757 ± 1.273 (81.693)	23.221 ± 3.024 (83.730)	18.694 ± 1.774 (81.075)	13.408 ± 1.196 (81.451)
heloc	6.564 ± 2.404 (77.430)	9.074 ± 3.894 (78.370)	5.504 ± 1.650 (77.968)	3.287 ± 0.758 (78.550)
house_16H	10.184 ± 2.667 (93.093)	17.963 ± 5.099 (93.351)	8.591 ± 3.370 (92.783)	3.937 ± 0.816 (93.058)
jannis	19.004 ± 1.246 (100.000)	22.482 ± 3.113 (100.000)	20.768 ± 2.200 (100.000)	12.008 ± 0.892 (100.000)
pol	16.267 ± 3.914 (98.348)	19.558 ± 5.785 (98.340)	17.384 ± 6.441 (97.883)	10.339 ± 2.743 (97.881)

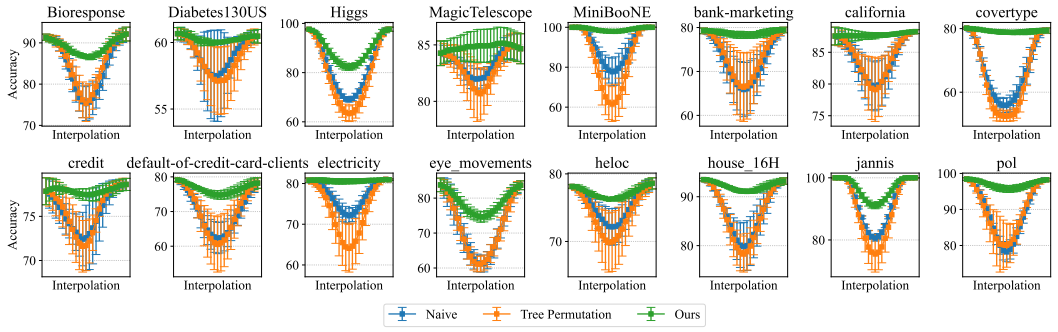

Figure 10: Interpolation curves of train accuracy for oblivious trees with AM.

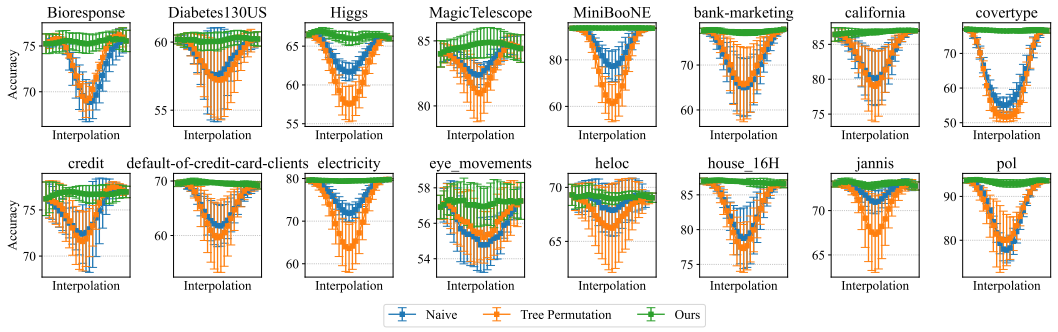

Figure 11: Interpolation curves of test accuracy for oblivious trees with AM.

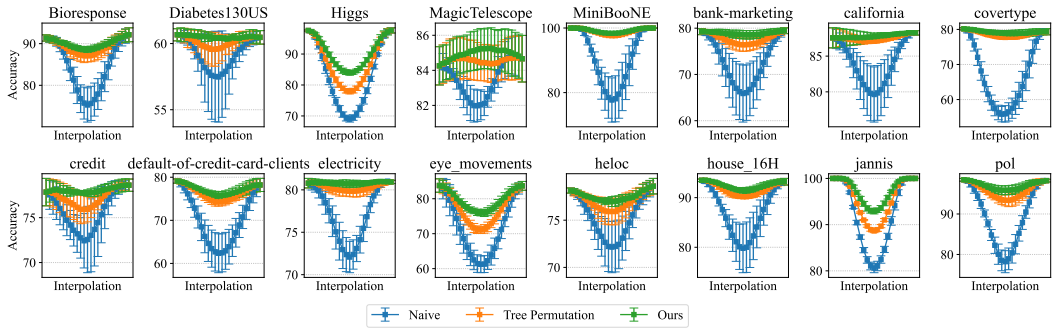

Figure 12: Interpolation curves of train accuracy for oblivious trees with WM.

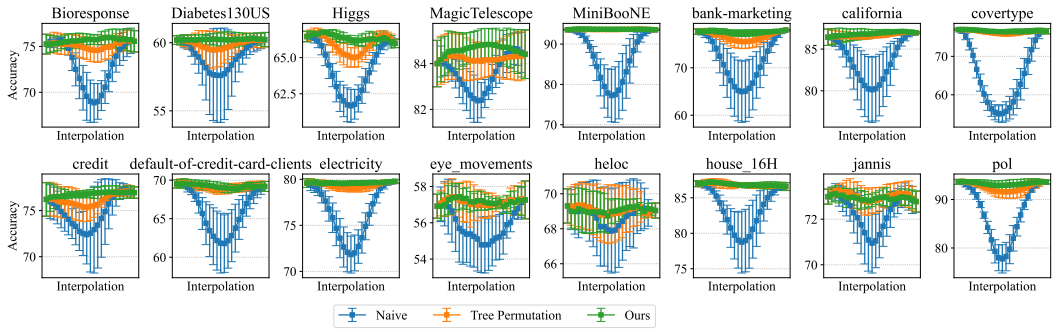

Figure 13: Interpolation curves of test accuracy for oblivious trees with WM.

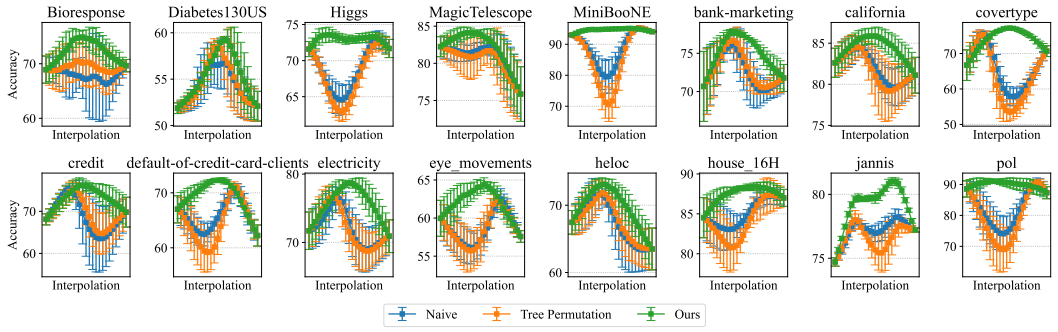

Figure 14: Interpolation curves of train accuracy for oblivious trees with AM by use of split dataset.

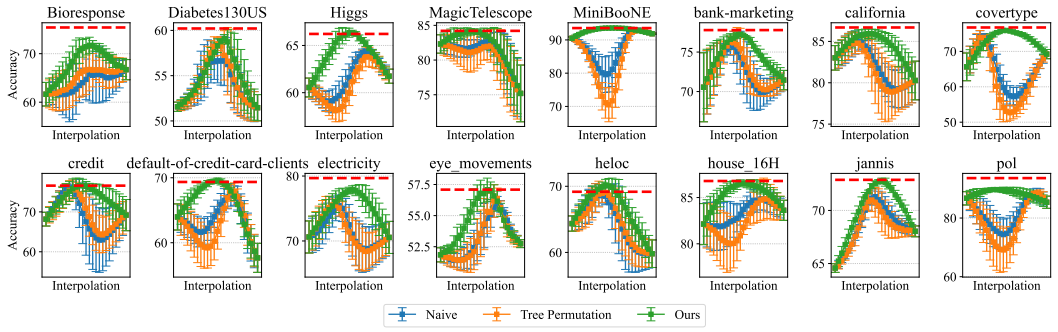

Figure 15: Interpolation curves of test accuracy for oblivious trees with AM by use of split dataset.

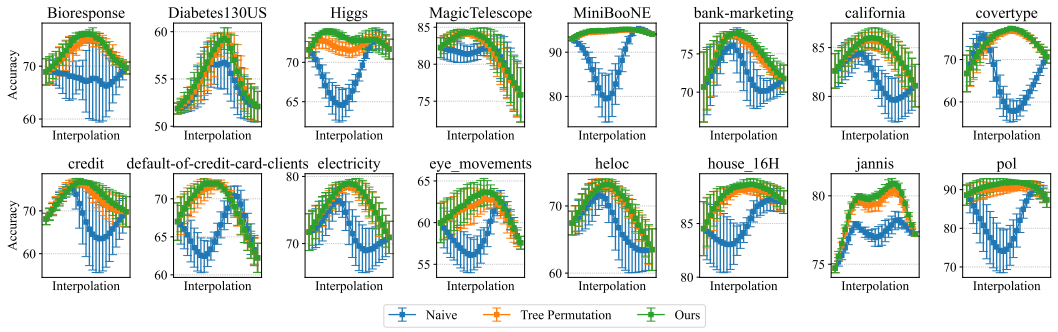

Figure 16: Interpolation curves of train accuracy for oblivious trees with WM by use of split dataset.

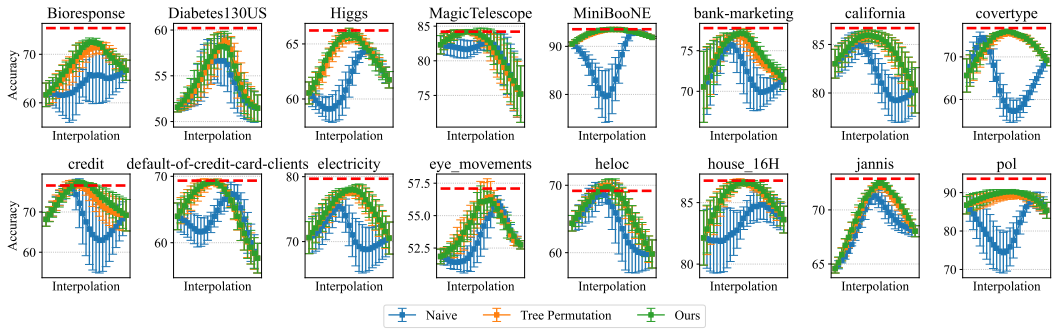

Figure 17: Interpolation curves of test accuracy for oblivious trees with WM by use of split dataset.

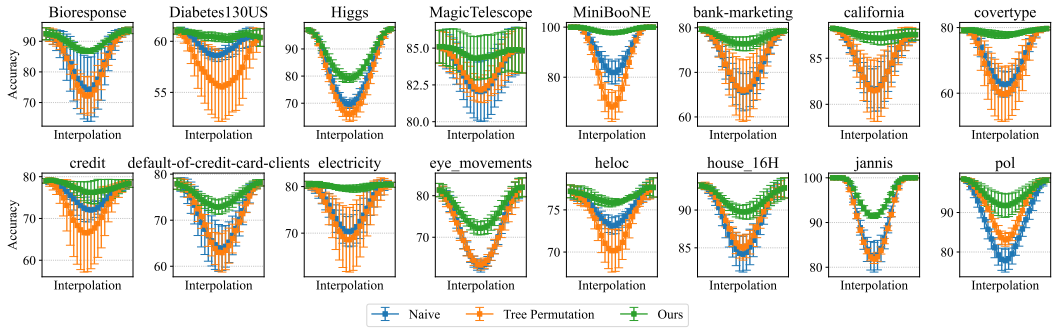

Figure 18: Interpolation curves of train accuracy for non-oblivious trees with AM.

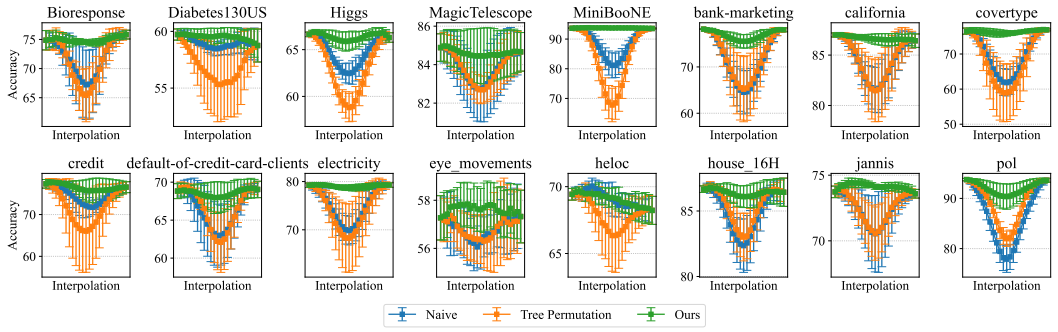

Figure 19: Interpolation curves of test accuracy for non-oblivious trees with AM.

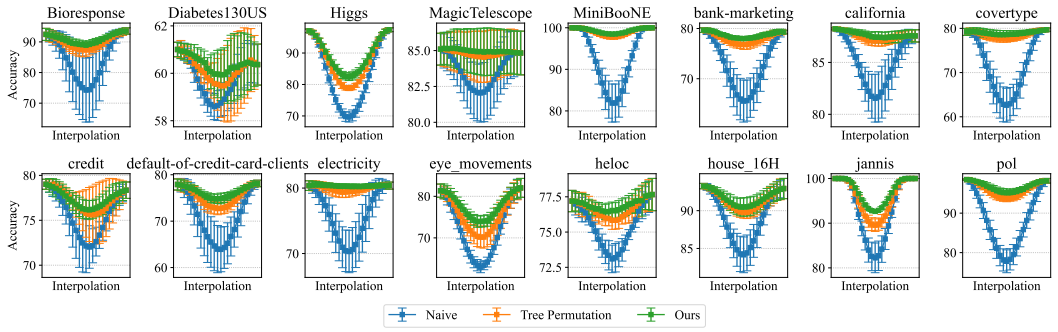

Figure 20: Interpolation curves of train accuracy for non-oblivious trees with WM.

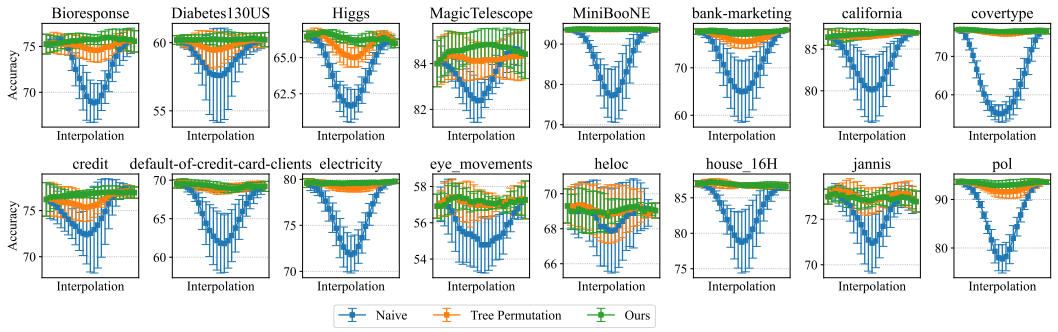

Figure 21: Interpolation curves of test accuracy for non-oblivious trees with WM.

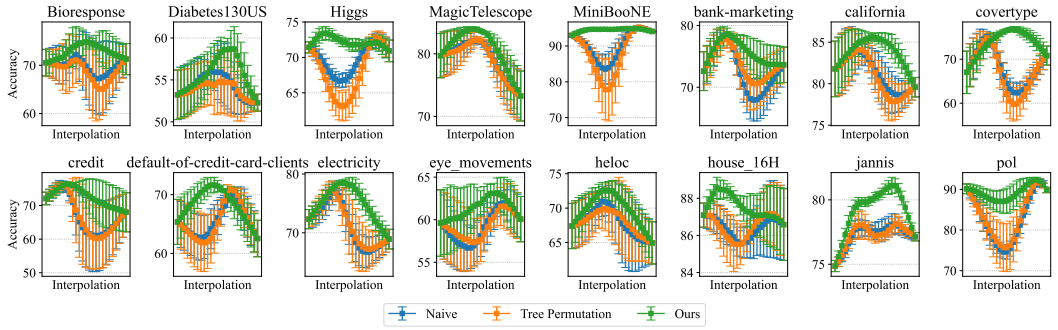

Figure 22: Interpolation curves of train accuracy for non-oblivious trees with AM by use of split dataset.

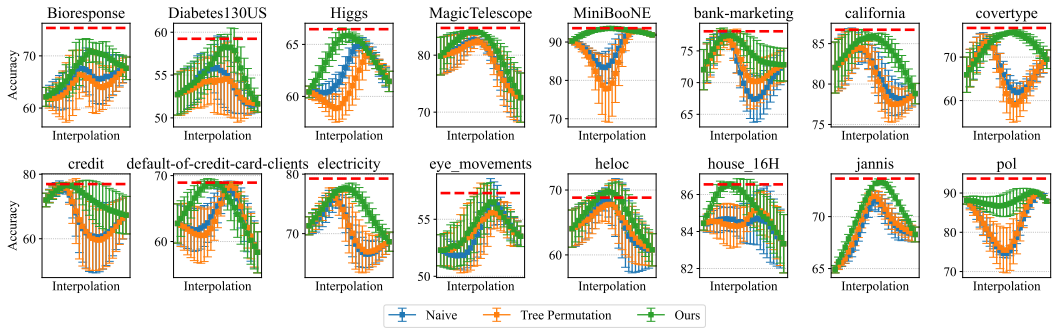

Figure 23: Interpolation curves of test accuracy for non-oblivious trees with AM by use of split dataset.

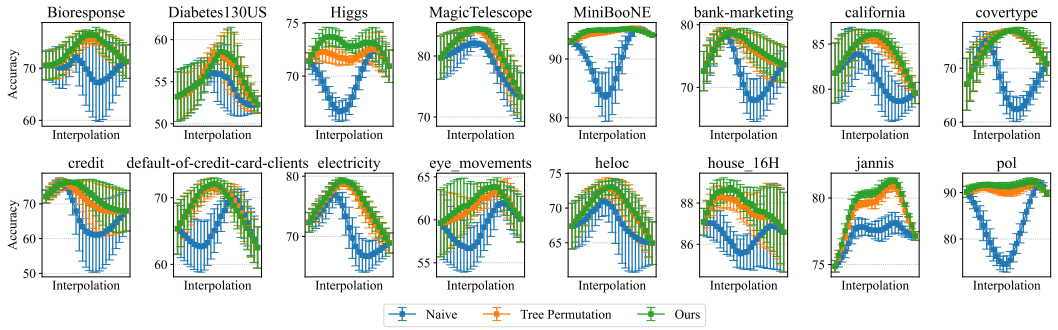

Figure 24: Interpolation curves of train accuracy for non-oblivious trees with WM by use of split dataset.

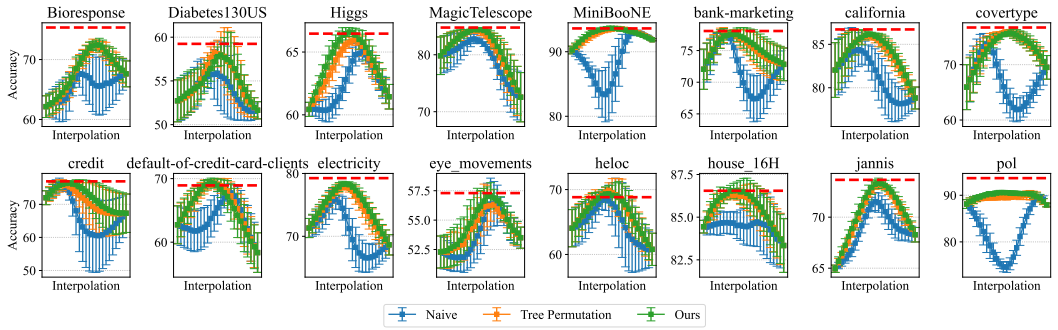

Figure 25: Interpolation curves of test accuracy for non-oblivious trees with WM by use of split dataset.

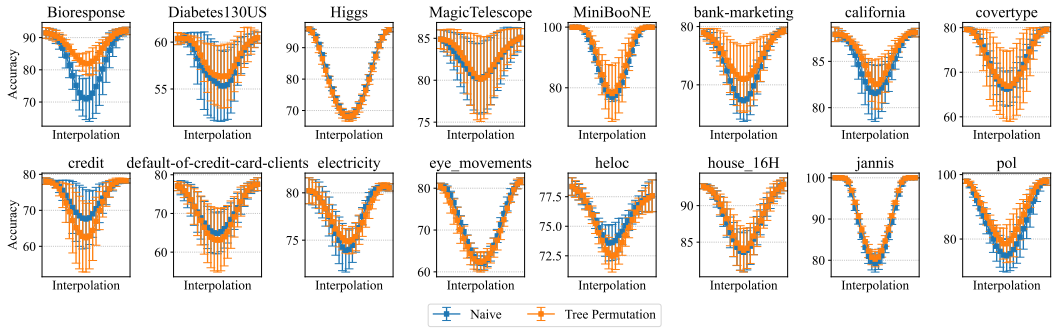

Figure 26: Interpolation curves of train accuracy for decision lists with AM.

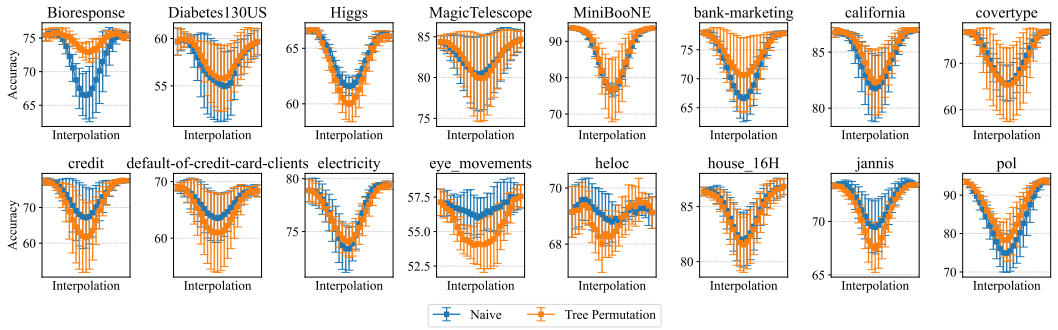

Figure 27: Interpolation curves of test accuracy for decision lists with AM.

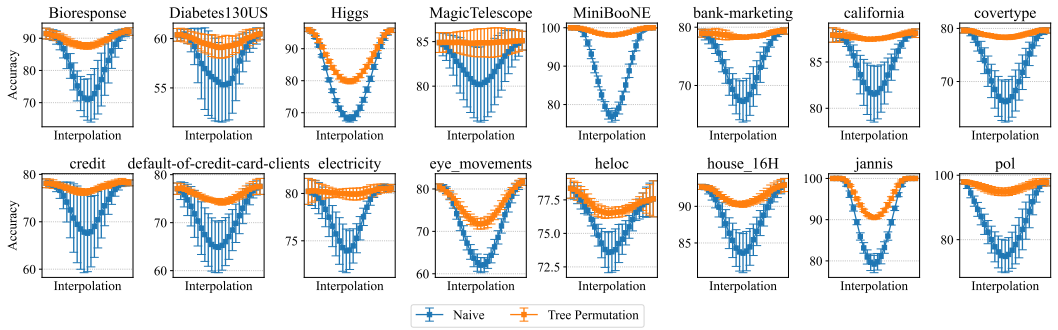

Figure 28: Interpolation curves of train accuracy for decision lists with WM.

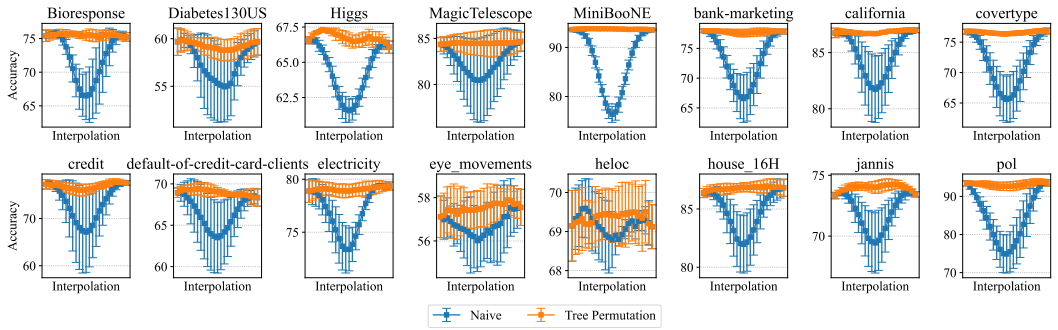

Figure 29: Interpolation curves of test accuracy for decision lists with WM.

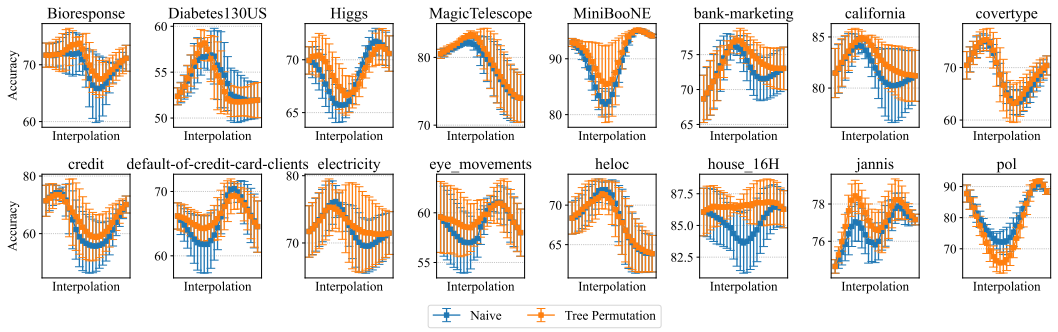

Figure 30: Interpolation curves of train accuracy for decision lists with AM by use of split dataset.

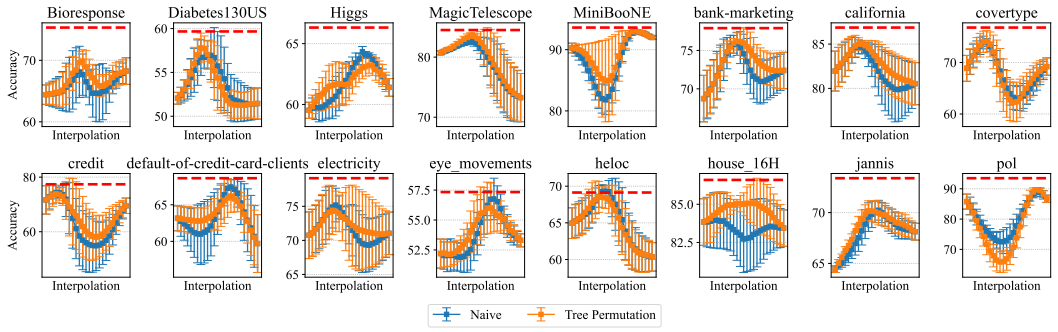

Figure 31: Interpolation curves of test accuracy for decision lists with AM by use of split dataset.

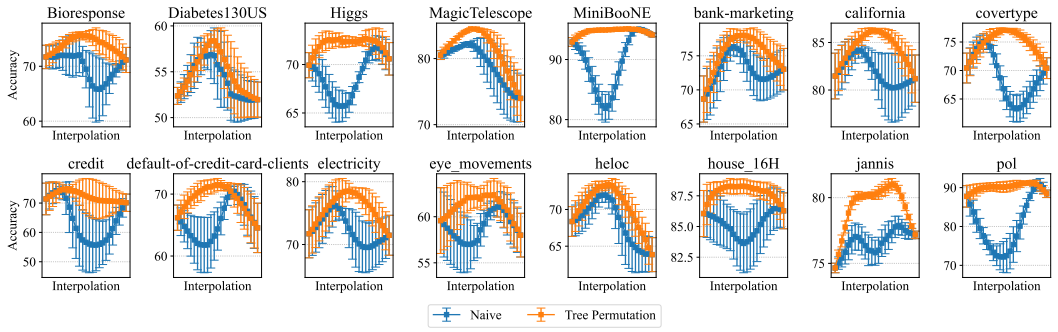

Figure 32: Interpolation curves of train accuracy for decision lists with WM by use of split dataset.

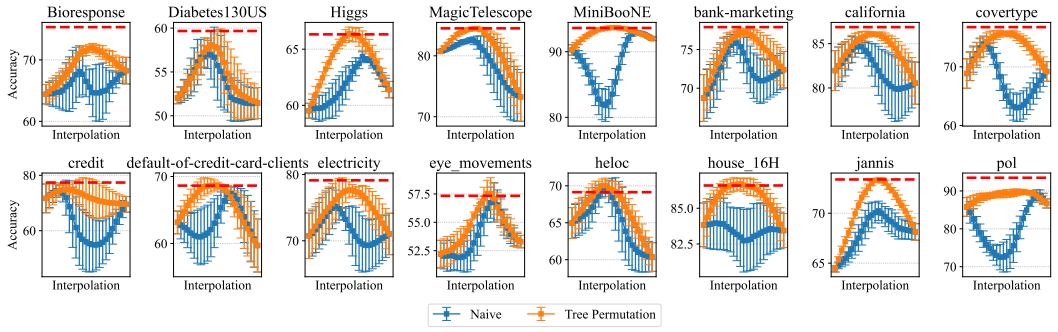

Figure 33: Interpolation curves of test accuracy for decision lists with WM by use of split dataset.

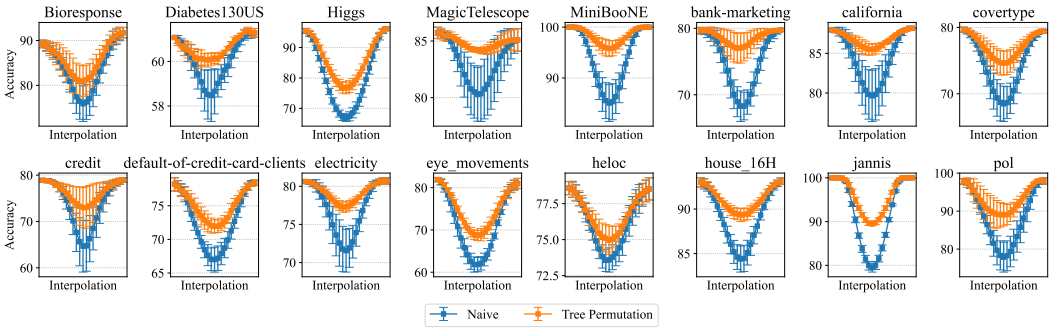

Figure 34: Interpolation curves of train accuracy for modified decision lists with AM.

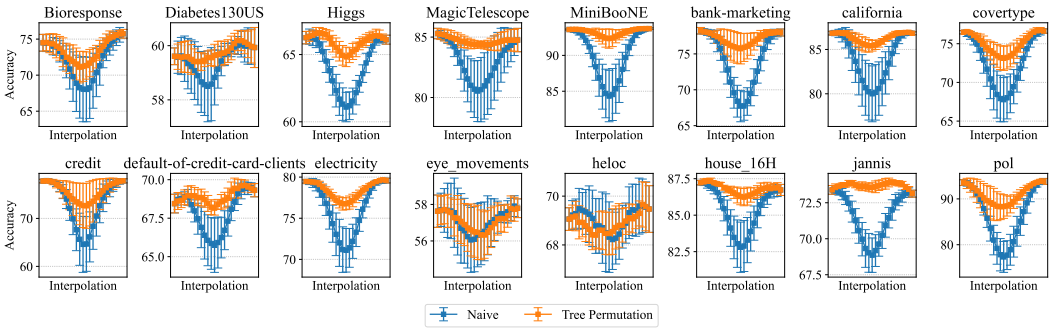

Figure 35: Interpolation curves of test accuracy for modified decision lists with AM.

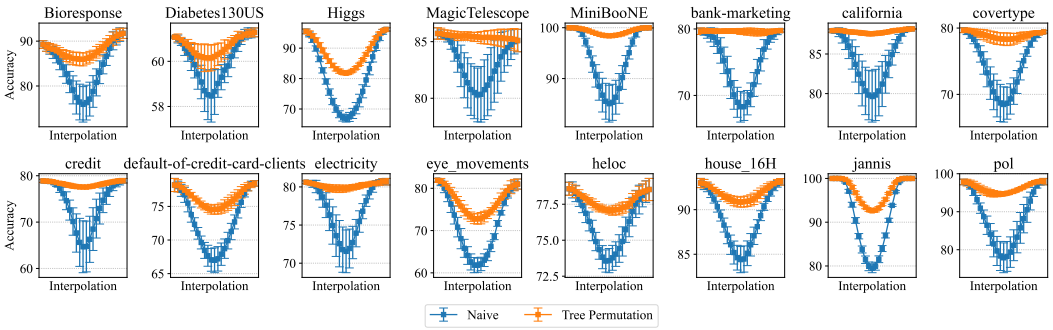

Figure 36: Interpolation curves of train accuracy for modified decision lists with WM.

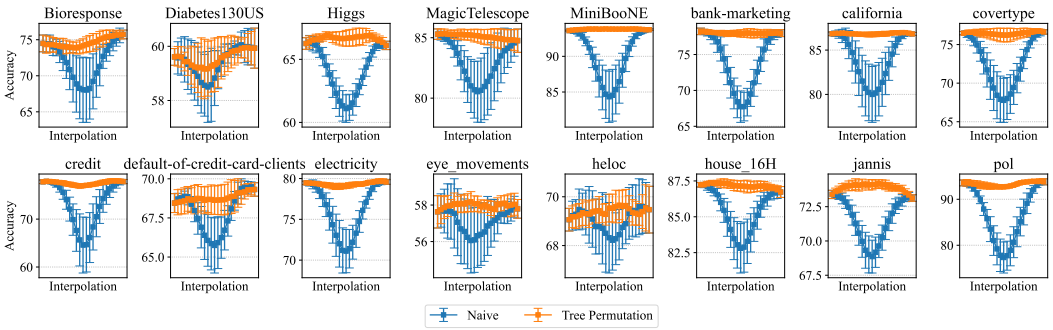

Figure 37: Interpolation curves of test accuracy for modified decision lists with WM.

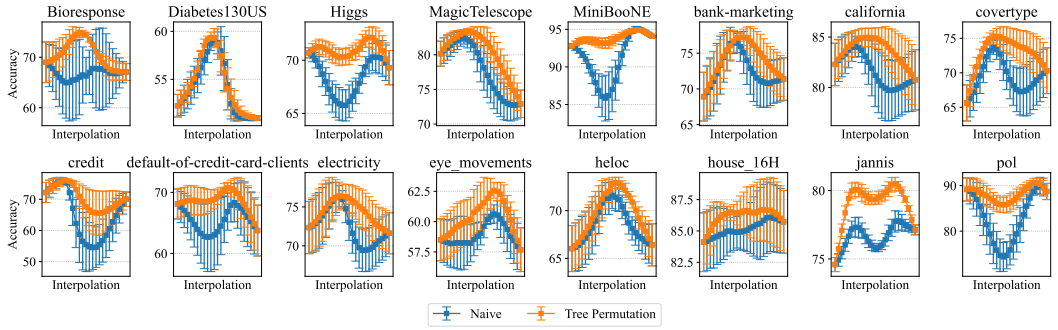

Figure 38: Interpolation curves of train accuracy for modified decision lists with AM by use of split dataset.

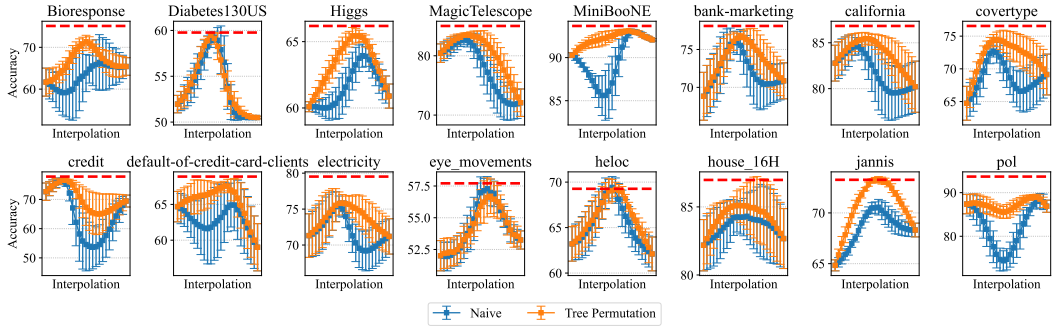

Figure 39: Interpolation curves of test accuracy for modified decision lists with AM by use of split dataset.

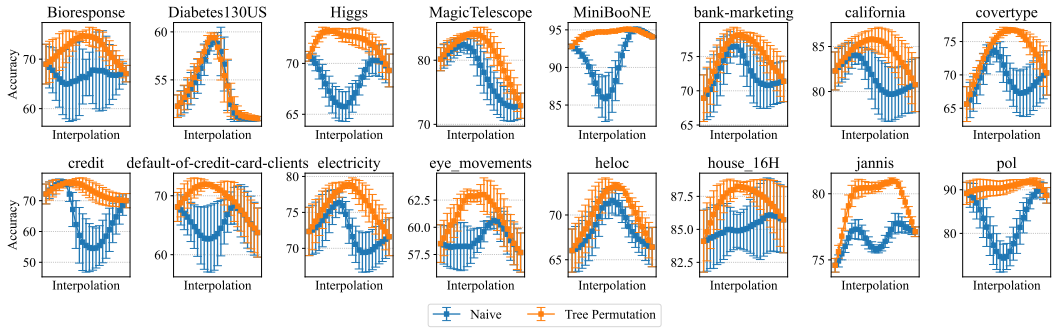

Figure 40: Interpolation curves of train accuracy for modified decision lists with WM by use of split dataset.

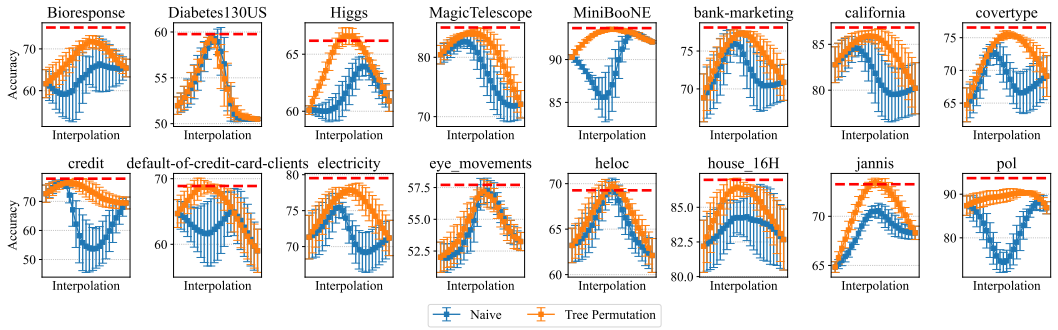

Figure 41: Interpolation curves of test accuracy for modified decision lists with WM by use of split dataset.

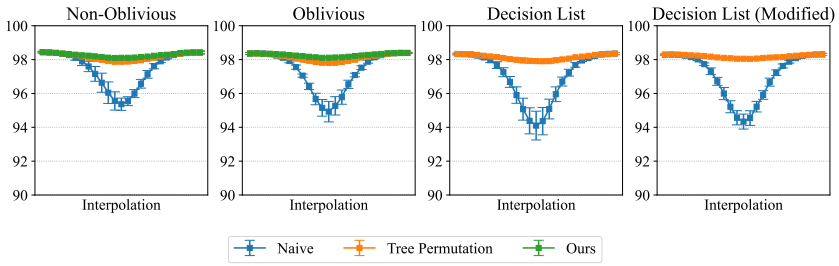

Figure 42: Interpolation curves of test accuracy with WM for MNIST (LeCun & Cortes, 2010) dataset.

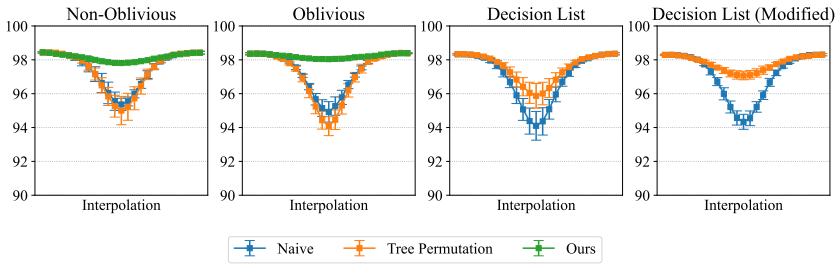

Figure 43: Interpolation curves of test accuracy with AM for MNIST (LeCun & Cortes, 2010) dataset.